Annu. Rev. Earth Planet. Sci. 2005. 33:571–604
doi: 10.1146/annurev.earth.33.092203.122604

First published online as a Review in Advance on January 18, 2005

PLANETARY SEISMOLOGY

Philippe Lognonné
Département de Géophysique Spatiale et Planétaire,
Institut de Physique du Globe de Paris, 94100 Saint Maur des Fossés, France;
email: lognonne@ipgp.jussieu.fr

Key Words Moon, Mars, interior, terrestrial planets

■ **Abstract** Contrary to Earth, the interior of terrestrial planets is poorly known. This is mainly related to the lack of seismic data and of planetary seismic networks on these planets. So far, despite several attempts, only the Apollo Seismic Network has returned seismic information from the Moon. But even in this case, very few seismic signals were recorded after a propagation path through the deep interior and core owing to a hemispheric distribution of the stations on the near side and to a probably strongly attenuating lower mantle. This review presents the main results achieved by the analysis of the Apollo seismic data and the associated constraints on the internal structure of the Moon. It then presents the current knowledge on the Martian interior, the seismic activity of the planet, and possible source of seismic noise. This information can be used for preparing future Martian seismic network missions. A short review on existing space-qualified instruments and on possible seismic missions toward other telluric bodies, such as Venus, the giant planets' satellites, or small bodies, is then given.

INTRODUCTION

Since the beginning of space exploration, successful missions performing planetary and small-bodies seismology have been limited to the Apollo program, with the deployment of a network of four seismic stations (Latham et al. 1969, 1970, 1971) in addition to the *Apollo 11* seismometer, which stopped operations after three weeks. The 12 other seismometers onboard launched missions never recorded any quakes. This includes the two Viking seismometers: Operators failed to unlock the first seismometer and the second one provided no convincing event detection after 19 months of nearly continuous operation (Anderson et al. 1977). The ten other instruments never reached their targets owing to the failure of their missions. These were the seismometers onboard the three Ranger lunar probes in the early 1960s (Press et al. 1960, Lehner et al. 1962), the *Apollo 13* seismometers, the two short-period seismometers onboard the Phobos 1 and 2 landers (Surkov 1989), and the two Optimism seismometers (Lognonné et al. 1998a) and the two short-period seismometers onboard the small surface stations (Linkin et al. 1998) and the penetrators of the Mars96 mission, respectively. For a historical review on

planetary seismology, excluding the Mars96 mission and other later attempts, see Toksoz (1975, 1979) and Lognonné & Mosser (1993). The latter also covered giant planet seismology, which is not addressed in this review.

Despite these discouraging records, international efforts for the deployment of seismometers on other terrestrial planets continue. The example of Mars shows indeed that most of the recent geochemistry theories in terrestrial planet formations or mineralogical models of Mars are unable to explain the few geophysical data gathered by the recent missions. The analysis and inversion of Martian seismic data will provide the first map of the seismic activity, as well as detailed models of the structure of the Martian crust, mantle, and core. They will therefore provide key constraints for assessing the validity of the planetary formation models, determining the types of material that have built terrestrial planets, and testing theories of planetary evolution.

This review focuses on the most recent results in planetary seismology of terrestrial planets. With the exception of the Moon, only a few pieces of geophysical information about the inner structure of the planets in the Solar System were returned from spacecraft explorations. For the deep interior structure of Mars, these are limited to the mean density, moment of inertia, and to one of the Love numbers characterizing the tidal response of the planet. The corresponding data are available also for the Moon, but no direct measure of the moment of inertia is available for all other telluric planets. The Moon case is therefore the only example where seismic data complement this basis information. It is presented in detail, with a description of the results of the Apollo seismic experiment from the 1970s and early 1980s and a detailed review of the works published more recently after new analysis of the Apollo seismic data (Vinnik et al. 2001; Khan & Mosegaard 2001; Lognonné et al. 2003; Nakamura 2003, 2004) or reanalysis of the Apollo travel times (Khan et al. 2000, Khan & Mosegaard 2002). For a more detailed review of the Apollo seismic experiment, see Toksoz et al. (1974), Lammlein et al. (1974), and Nakamura (1983). I then draw the present view of the Moon interior obtained from the joint analysis of these results with other geophysical and geochemical data. For Mars, I first review the present knowledge of the interior structure and describe the perspective of future missions performing seismic exploration. The a priori description of the seismic activity, seismic noise, and seismic propagation properties is first given and then exploration strategy is detailed, including future programmatic issues and instrumentation constraints. The state of the art in the development of space seismometers is briefly presented. I finally present future challenges in planetary seismology, first for the Moon and Mars, and then for Venus, the Jovian satellite Europa and small bodies.

LUNAR SEISMOLOGY

The Apollo Seismic Experiment

The first seismometer working on a planetary body other than Earth was installed in July 1969 by the *Apollo 11* crew (see instruments details in Latham et al. 1969).

It was a package of two seismometers: a three-axis long-period (LP) and a short-period (SP) vertical axis. Both had peaked sensitivities of 5×10^{-11} m in ground displacement at 0.45 Hz and 8 Hz for the LP and SP respectively. The *Apollo 11* package was operated by solar panels and worked for 21 Earth-days, excluding the night-time stand-by. It stopped during the second lunar day, 37 days after the initial activation (Latham et al. 1969, 1970). Later, with the other Apollo missions, a network of four seismometers, continuously powered by a radioactive thermal generator, was deployed and turned off from the Earth in September 1977. The huge amount of data collected during the 26.18 active station years is now available in raw format in the Data Center of the Incorporated Research Institutions of Seismology (IRIS) (http://www.iris.edu/data/data.htm) and also in the author's institution data center, in a Standard for the Exchange of Earthquake data (SEED) (http://ganymede.ipgp.jussieu.fr/GB/donnees/; Gagnepain-Beyneix et al. 2002). Remote recorded seismic events are either impacts (meteoroids and artificial impacts) or quakes [deep and shallow, the later named High Frequency Teleseismic (HFT) events]. Local events, called thermal Moonquakes, were also recorded after sunrise or sunsets, probably generated by near surface thermal cracks and deformations (Duennebier & Sutton 1974). During the seven years of the Apollo Seismic Network operation, approximately 12,500 seismic signals were detected on the LP instruments and cataloged, and many times more remain uncataloged with the SP instruments. The most recent LP catalogue of events is available on line at the University of Texas at ftp://ig.utexas.edu/pub/PSE/catsrepts (Nakamura, 2004).

Figure 1 shows a typical example of deep Moonquake records. Their depth ranges from 700 km to 1000 km, and they occur repeatedly on a small number of distinct foci, with periodicity related to the Moon orbit perturbations, especially periods of 27, 206 days, and 6 years. Latham et al. (1971), Lammlein (1977), Cheng & Toksöz (1978), and Goins et al. (1981a) performed detailed analysis of these events, in terms of magnitude, location, stress drop, and proposed mechanism. They have shown that the maximum amplitude of the Moonquakes is typically of only a few digital units on the LP records; initial polarity appears to be correlated with the tidal cycle (Lammlein 1977); and that the largest deep Moonquake nest in terms of magnitude, the A1 site, releases events with a seismic moment of approximately 5×10^{13} Nm, characterized by a corner frequency of approximately 1 Hz and a stress drop of 0.1 bar. Further source studies have shown that the radiation patterns of deep Moonquakes from a single source region were rotating with changes in tidal stress (Nakamura 1978). By using single-link cluster analysis, Nakamura (2003) recently increased the number of detected deep Moonquake signals to more than 7200. More than 160 Moonquake epicenters have been found and associated with signals observed at several Apollo stations, and this number might increase with further studies, especially with the search for deep Moonquakes originating from the far side of the Moon (Nakamura 2004, Oberst & Mizutani 2003). Stacking methods have been used to generate better seismograms from all events originating from a given source (see Figure 1 for stacked data), not only in the original studies (e.g., Nakamura 1983) but also in recent studies (Lognonné et al. 2003, Nakamura 2003). Detailed analysis, however, shows that the events have slightly

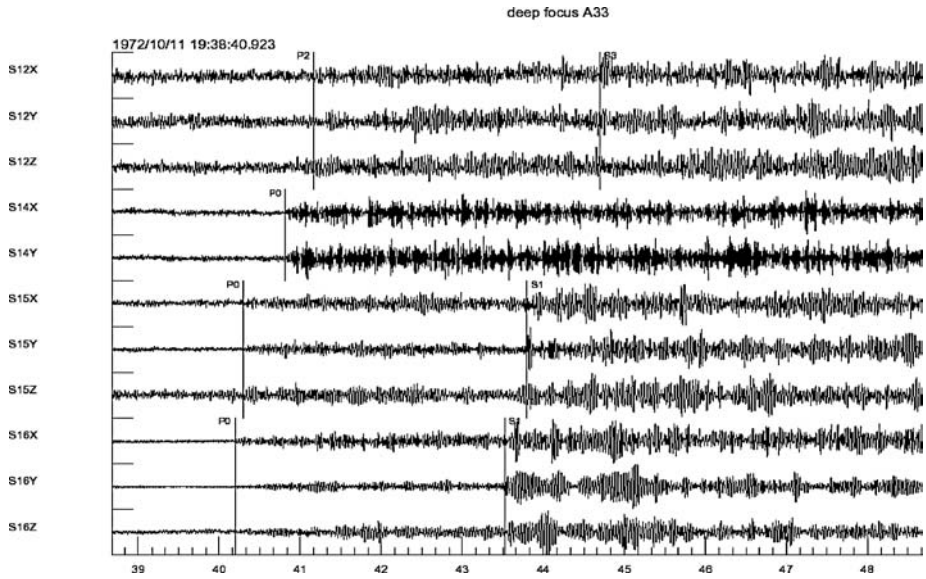

Figure 1 Stacked seismograms for the A33 deep Moonquake source and for all Apollo stations. Arrivals of P and S waves identified after stacking are plotted. The number is associated with the error range in the arrival time picking. 0, 1, 2, and 3 are for errors below 1 s, 3 s, 10 s, and 30 s, respectively.

different epicentral positions, and that stacking methods are less efficient for the SP data.

Figure 2 (see color insert) shows the compilation of the natural impacts, whereas an example of artificial impact is shown in Figure 3. In addition to providing information on the internal structure, these events have been used for the determination of the orbital characteristics of the meteoroid impacting the Moon (Oberst & Nakamura 1987, 1991), and the mass of the meteoroid has been estimated (Oberst & Nakamura 1991, Lombardi et al. 2002). The last signals are the HFT Moonquakes: They are much stronger (Nakamura 1977b), but only 28 such events were observed during the nearly 8 years of network operation.

The seismic data show an intense scattering and reverberation in the crust and subsurface. This is characterized in the records by very long reverberations and coda for the P and S waves and a slow decrease of the amplitude during several tenths of minutes (Figure 3). An exact description of the scattering process from the elastic wave equation is extremely difficult, and thus only approximations have been used, such as the diffusion theory (Dainty et al. 1974; Nakamura 1976, 1977a). Both experiments (Dainty et al. 1974) and observations (Toksoz et al. 1974) show that the scattering zone, probably related to the fracturation of the crust, must be located within a near surface zone between 1 and 20 km thick, and below 20 km, the scattering is much weaker. Nakamura (1977a) has, however, shown

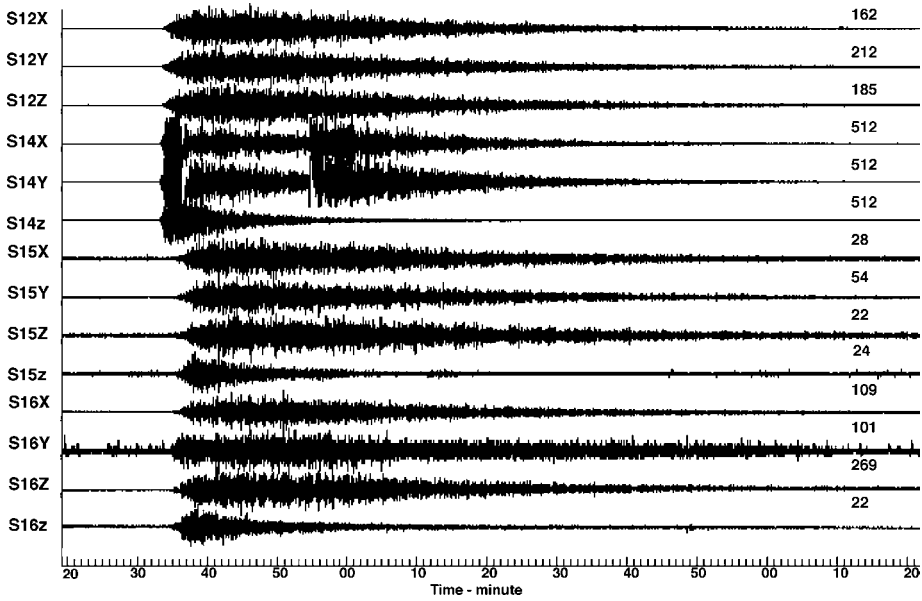

Figure 3 Seismic records from the Apollo Seismic Network of the impact of the *Apollo 17* Saturn V upper stage (Saturn IVB) on the Moon on December 10, 1972, at distances of 338, 157, 1032, and 850 km from the *Apollo 12*, *14*, *15*, and *16* stations, respectively). X, Y, and Z are the long-period seismometers; z is the short-period seismometer. These amplitudes are mainly related to S waves trapped in the regolith. The first P arrival is typically 10 times smaller. The X and Y channels of the *Apollo 14* station were operated at –10db gain at the time of the impact and have amplitudes decreased by 3.16 as compared to other channels with the nominal gain. Numbers at the right are peak amplitudes in digital units.

that the size distribution of scatters is very close to those of craters on the Moon, and that cratering is probably one of the principal causes of scattering by creating irregularities of the surface and associated subsurface faults. Only few attempts to model these waves have been done, mainly owing to the lack of available models; however, techniques based on normal mode summation, even up to frequencies of 0.3 Hz, can provide rough estimates of the mean amplitudes of the P and S pulses. With artificial impacts (for which the amplitude of the source is known), the mean amplitudes of synthetics are typically found within 20%–30% of those of the data (Lombardi et al. 2002).

The very low quake's magnitude and the intense diffraction on the Moon require very sensitive broadband LP instruments to record waves with wavelengths comparable or larger than the crust. However, the broadband mode of the LP seismometers, despite a flat response in displacement between 1 s and 20 s, was much less sensitive ($2–3 \times 10^{-10}$ m in ground resolution) and more noisy than the peaked mode and was therefore rarely used. This lack of broadband

performances has severely limited the analysis of the seismograms. Practically, with the exception of crustal phases, tentatively identified on single records by Toksöz et al. (1972a,b) and Goins et al. (1981b), only direct P and S arrival times have been used for the determination of seismic models and the waveforms have been rarely used. Eighty one sources were compiled and used at the end of the experiment for global seismic velocity inversion by Nakamura (1983), with 18 meteoroids impacts, 8 artificial impacts, 14 shallow events, and 41 deep Moonquakes. All the theoretical 324 P or 324 S arrival times were not determined, and these 81 sources provided only 203 P and 243 S measured arrival times. When the origin time and locations coordinates of the sources, unknown for all but the artificial impacts, are subtracted from the number of data, 172 degrees of freedom remain available for the internal structure. Due to the probable presence of a few bad picks in this data set (Khan & Mosegaard 2002, Nakamura 2003) and of data with large errors (sometimes more than a few tens of seconds between different author's readings), Lognonné et al. (2003) give a new arrival time picking with data's individual error estimates and select 59 events with the smallest errors (19 natural impacts plus the *Apollo 16* S-IVB impact, for which both the time and location of impact are unknown due to telemetry lost, 7 artificial controlled impacts, 24 deep Moonquakes, and 8 shallow quakes). This data set has a mean error of approximately 2 s and is leading to 183 P and 136 S arrival times and to 131 degrees of freedom for internal structure. For the 142 common arrival times between Nakamura (2004) and Lognonné et al. (2003), a root mean square difference of 6.8 s is found when all data are equally weighted and only 2.8 s is found when the weight proposed by Lognonné et al. (2003) is used, showing the importance of weighted data. Other studies were done with the same data set as Nakamura (Khan et al. 2000, Khan & Mosegaard 2002) or with fewer events, as for Goins et al. (1981c), who have used 40 events (8 natural impacts, 8 shallow quakes, and 24 deep Moonquakes), or for Koyama & Nakamura (1979), who used 25 events. The low number of degrees of freedom for internal structure (131–172) and the low quality of the data are the main limitations in the proposed models of the Moon interior. This leads to a large tradeoff between depth resolution and a posteriori uncertainties, as discussed below.

Subsurface and Crustal Thickness Determination

In the subsurface, very low seismic velocities are observed due to the lunar regolith, a loose particulate rock material layer produced by the impacting history on the Moon surface (see Cooper et al. 1974 for a review). This low velocity zone produces an amplification of SP seismic waves by reverberations and a loss of the seismic pulse coherency. The subsurface structure has been studied with active seismic experiments on the 14, 16, and 17 sites (Cooper et al. 1974); with the passive seismometers and signal of the lunar module lift-off at the 12, 14, and 15 sites (Nakamura et al. 1975); by frequency analysis of the horizontal-to-vertical amplitude ratio of natural events at the 12, 14, 15, and 16 sites (Horvath et al. 1980); and, finally, with the receiver function method at the 12 landing site (Vinnik et al. 2001).

The first 10 to 20 m have shear velocities below 100 m/s, whereas S velocities higher than 300 m/s are found deeper than 100–200 m. Such structures are producing resonances at frequencies higher than 1–2 Hz, making the analysis of arrival times difficult. A large V_p/V_s of approximately 1.9 ± 0.3 is found near the surface and a more classical value of 1.70 ± 0.04 is found at the base of the crust. Below these layers and up to 1–1.5 km, a layer with V_p from 1000 to 2000 m/s was generally found, interpreted as a fractured and broken zone extending to more concrete crustal materials, where V_p rises, respectively, up to 4.7–4.9 km/s (Cooper et al. 1974, Nakamura 1983). The *Apollo 12* landing site has the smallest thickness of regolith (Horvath et al. 1980, Mark & Sutton 1975) and is of particular interest for the future Japanese Lunar-A mission, which will deploy one of its two penetrators in its vicinity (see section on Planned Missions). Vinnik et al. (2001) suggested that the high-velocity basement (i.e., shear velocities higher than 1000 m/s) at station 12 should be approximately 150 m deep, a depth twice smaller than the one proposed by Mark & Sutton (1975). A correlation between the horizontal components of motion at station 12 was also found, with a stable polarization of the waves with a -60° North azimuth, pointing out toward the 100 km near-Lansberg impact crater (42 km in diameter) (Vinnik et al. 2001, Chenet 2003), which might be explained by reverberations between the impact-generated fractures.

The volume of the lunar crust is directly related to the depth of the post-accretional magma ocean and the efficiency of the primary crust differentiation. Moreover, owing to the concentration of radiogenic elements in the crust, its thickness should strongly constrain the bulk inventory of U and Th of the planet (e.g., Taylor 1986). Its determination is therefore a key objective of seismology. A thickness of 65 km was proposed after the pioneering work of Toksöz et al. (1972a,b) and developed later by Toksöz et al. (1974). But this estimate has been questioned recently in the works of Khan et al. (2000), Khan & Mosegaard (2002), Chenet (2003), and Lognonné et al. (2003), who have independently proposed a much thinner crust. Using the same data as Nakamura (1983), Khan & Mosegaard (2002) performed a Monte-Carlo inversion. They obtained a rapid increase between the surface and 20 km and then a slower increase down to a 40 km discontinuity (Figure 4*a*, see color insert). After an earlier estimate of 45 ± 5 km (Khan et al. 2000), they considered a shallower crust-mantle boundary, approximately 38 ± 3 km deep, to be four times more likely than a discontinuity between 50 and 70 km deep. Lognonné et al. (2003), in a study later detailed and improved by Gagnepain-Beyneix et al. (2004) (J. Gagnepain-Beyneix, P. Lognonné, H. Chenet, D. Lombardi, T. Spohn, submitted manuscript), have found a velocity increase at a depth of approximately 30 km. The used data were direct P and S waves travel times and the differential travel time of S to P crustal converted phases obtained from a receiver function analysis (Vinnik et al. 2001). No major discontinuity at 45 or 58 km, compatible with both the travel times and the amplitude of the S and P converted phase (Figure 4*b*) was found. By taking into account the crustal lateral variations, Chenet (2003) and Chenet et al. (2004) obtained a mean crustal thickness on the near side, in the Procellarum KREEP Terrane (PKT), of 34 ± 5 km,

a value closer to the depth observed by Khan & Mosegaard (2002), who take some of the lateral variations into account by inverting a delay time at all Apollo stations.

These recent estimates are therefore significantly smaller than the original 65 km, a value also challenged by Koyama & Nakamura (1979) with a 45 km crustal thickness from a global inversion of travel times, explained mainly by smaller velocities in the lower upper mantle ($V_p = 7.85 \pm 0.04$ km/s, $V_s = 4.31 \pm 0.03$ km/s) as compared to previous results ($V_p = 8.10$ km/s, $V_s = 4.70$ km/s). The main argument used in the Toksöz et al. (1972a) paper, with its 60 km value estimation, was the amplitude amplification at an epicentral distance of approximately 170 km. Toksöz et al. (1972a,b) explain this amplification by a ray focusing at this distance. Their interpretation, already discussed by Khan & Mosegaard (2002), is however strongly dependant on the velocity value used below the boundary, and values as high as 8.9 km/s were necessary. But as noted in the note added in proof of Toksöz et al. (1972a), "The first detectable motion at the *Apollo 15* seismometer indicates an average velocity of at least 8 km/s near a depth of 130 km. Whether the high velocity (9 km/s) zone in the uppermost portion of the mantle (reported above) is a universal feature or not cannot be determined from the new data." None of the further studies have found such high values, and only velocities either in the range 7.6–7.9 km/s (Goins et al. 1981, Nakamura 1983, Lognonné et al. 2003) or in the range 8.0 ± 0.8 km/s (Khan et al. 2000, Khan & Mosegaard 2002) were reported.

The comparison of the different seismic V_p models with those extrapolated from the lunar samples, as shown in Figure 4*b,* may support models with smaller velocities in the crust. The Toksöz (1974) values and even the Khan & Mosegaard (2002) values appear to be high with respect to experimental ones, in opposition to values proposed by Lognonné et al. (2003), more in the range of the crustal velocities extrapolations. Further seismic investigations are however needed to confirm in-situ such values, as well as works on the impact of the trade-off between the seismic velocity profile in upper crust and the mean crustal thickness. However, a depth ranging from 30 to 45 km in the PKT from the more recent reprocessing or inversion of the Apollo seismic data is challenging the previous crustal thickness determinations. Such a range is also supported by other seismic arguments, such as the lunar mantle temperature as constrained by the lunar upper mantle seismic data (Lognonné et al. 2004).

The Moon Mantle: A Pyroxenite Upper Mantle with a Primordial Lower Mantle?

Figure 5 (see color insert) shows the different seismic models of the mantle, found by various studies, with values summarized in Table 1. Two approaches were chosen: The first is an inversion for a model with only a few layers and generally for both V_p and V_s (Goins et al. 1981c, Nakamura 1983, Lognonné et al. 2003). Typically, 3–4 layers have been inverted in the mantle and 4–6 layers in the crust, leading to approximately 20 parameters in the inversion, as compared to 130–160 degrees of freedom of the data set. Such an approach reduces the number of

TABLE 1 Comparison of the different seismic models of the Moon for area II, III, and the top-most part of IV with geochemical constraints provided by Kuskov et al. (2002) for the same area

Depth (km)	Goins et al. (1981c)	Nakamura (1983)	Lognonné et al. (2003)	Gagnepain-Beyneix et al. (2004)	Khan & Mosegaard (2002)	Kuskov et al. (2002)
Crust–300[a]	4.47 ± 0.05	4.49 ± 0.05	4.53 ± 0.15	4.44 ± 0.04	4.0 ± 0.4	4.51 ± 0.18
	7.70 ± 0.15[f]	7.74 ± 0.12	7.75 ± 0.15	7.65 ± 0.06	8.0 ± 0.8	7.81 ± 0.40
300–500[b]	4.37 ± 0.05	4.25 ± 0.10	4.50 ± 0.15	4.37 ± 0.07	4.0 ± 0.4	4.42 ± 0.19
	7.65 ± 0.15[g]	7.46 ± 0.25	7.75 ± 0.15	7.79 ± 0.12	8.0 ± 0.8	7.85 ± 0.40
500–620[c]	4.20 ± 0.10	4.65 ± 0.16	4.35 ± 0.30	4.40 ± 0.11	5.4 ± 0.9	4.44 ± 0.20
	7.60 ± 0.60	8.26 ± 0.40	7.50 ± 0.30	7.62 ± 0.22	9.9 ± 1.9	8.01 ± 0.38
620–750[d]	4.20 ± 0.10	4.65 ± 0.16	4.35 ± 0.30	4.40 ± 0.11	5.5 ± 0.9	4.44 ± 0.20
	7.60 ± 0.60	8.26 ± 0.40	7.50 ± 0.30	7.62 ± 0.22	9.0 ± 1.9	8.01 ± 0.38
750–1000[e]	4.20 ± 0.10	4.65 ± 0.16	4.20 ± 0.30	4.50 ± 0.10	6.0 ± 0.7	4.44 ± 0.20
	7.60 ± 0.60	8.26 ± 0.40	7.90 ± 0.30	8.15 ± 0.23	11 ± 2.1	8.01 ± 0.38

All seismic velocities are in km/s.

[a]Depth is 270 for Nakamura (1983), 238 km for Gagnepain-Beyneix et al. (2004).

[b]Maximum depth is 488 km for Gagnepain-Beyneix et al. (2004) and 560 km for Khan & Mosegaard (2002).

[c] Depth range is 560–620 km for Khan & Mosegaard (2002).

[d]Maximum depth is 738 km for Gagnepain-Beyneix et al. (2004) and depth range is 620–780 km for Khan & Mosegaard (2002).

[e] Depth range is 780–1100 km for Khan & Mosegaard (2002).

[f]Velocity at 230 km deep.

[g]Velocities at 480 km deep.

parameters of the inversion and takes into account the low sensitivity of travel times to gradients. It leads to the determination of the mean velocity in each layer while reducing the a posteriori error by approximately $\sqrt{(130/20 - 160/20)} = \sqrt{(6 - 8)}$, as compared to the a priori errors associated with the travel time readings and mislocation of the events. In contrast, Khan et al. (2000) and Khan & Mosegaard (2002) used many more layers (56 with the two V_p and V_s parameters) and a Markov Chain Monte Carlo technique for the inversion. Larger errors in the a posteriori velocities are found, leading to weaker constraints in terms of mineralogy (Figure 5). Moreover, as noted by Kuskov et al. (2002), the velocities with the highest marginal probabilities shown in Figure 5 are not within the range of seismic velocities obtained by mineralogical considerations. We therefore mainly discuss the seismic values of the Goins et al. (1981c), Nakamura (1983), Lognonné et al. (2003), and Gagnepain-Beyneix et al. (2004) models, and use the results of Khan & Mosegaard (2002) for the relative variations of velocities with depth.

These models agree fairly well in the upper mantle (i.e., the first 300 km in depth), with a mean value of 4.47 km/s and 7.70 km/s between the three models, and maximum differences of 0.05 km/s and 0.10 km/s, comparable to the proposed errors. Deeper, Nakamura's model shows a strong decrease of both V_p and V_s velocities, with a low velocity zone between depths of 270 km and 500 km. Such a feature is not observed in the models of Goins et al. (1981c), Lognonné et al. (2003), and Gagnepain-Beyneix et al. (2004), but as discussed by Nakamura (1983), this variation is purely a consequence of parameterization, and could very well be a gradual decrease without any sharp discontinuity. No decrease is observed for P velocities by Khan & Mosegaard (2002) either in the upper mantle with quite constant velocities in the mantle, down to a depth of 500 km. A minor S velocity decrease is, however, found between depths of 280 km and 320 km.

An increase of the seismic velocities is found by Nakamura (1983) at a depth of 500 km and by Gagnepain-Beyneix et al. (2004) at a depth of 738 km. Khan & Mosegaard (2002) also found an increase of velocities in the lower mantle, but large uncertainties are found for P down to 800 km depth. More constrained S velocities are, however, found at a depth of 550 km. This increase in the seismic velocities is probably the signature of a transition between the upper and the lower mantle. But more data will be necessary to obtain an accurate depth estimate (in the case of a rapid discontinuity) or the depth and extension of the gradient zone (for a more gradual discontinuity), as pointed out by Hood (1986) and by Lognonné et al. (2003), who have shown that the inverted values at this depth are constrained mainly by a few rays. Such poor resolution of the structure between 400 km and 800 km depth probably explains the absence of a clear maximum in the marginal probabilities of P velocities found by Khan & Mosegaard (2002).

These models have led to several interpretations in terms of mantle mineralogy. Whereas Buck & Toksöz (1980) discussed earlier results, Hood & Jones (1987), Mueller et al. (1988), Kuskov (1995, 1997), Kuskov & Fabrichnaya (1994), and Kuskov & Kronrod (1998) discussed mainly the Nakamura (1983) model. Hood & Zuber (2000) and Kuskov et al. (2002) interpreted the models of Nakamura (1983)

and Khan et al. (2000). Lognonné et al. (2003) provided a mineralogical interpretation of their models based on Kuskov's papers. In the upper mantle, as noted by Kuskov (1995) and Lognonné et al. (2003), these velocities are compatible with pyroxenite compositions. Two possible compositions, with rather different FeO proportions (13.8% and 17.6%) and Mg numbers of 75 and 72, respectively, fit the seismic velocities fairly well. The first was proposed by Ringwood & Essene (1970) as a possible source of mare basalt originating from depths of 200–500 km. The second was proposed by Kuskov (1995) to explain the lower bound of the Nakamura model. If both fit the seismic velocities, the density of the second is too high to fit the density constraints of the upper mantle given by the inertia factor and mean density. In contrast, both the geochemical (Taylor 1987) and the geophysical arguments support the first composition (i.e., FeO approximately 13% and Mg number of 75).

The increase in velocity, found deeper by Nakamura (1983), Gagnepain-Beyneix et al. (2004), and Khan & Mosegaard (2002), has been interpreted as the signature of a discontinuity in the composition of the Moon mantle, separating an upper differentiated mantle from a lower primordial mantle. Nakamura (1983) proposes a depth of 500 km and Khan & Mosegaard (2002) propose 560 $\pm$ 15 km. For Gagnepain-Beyneix et al. (2004), the data are too sparse to distinguish a gradual increase of the velocity between 400 and 750 km from a discontinuity. Hood & Jones (1987) and Mueller et al. (1988) proposed an increase in the Mg number in this transition zone relative to the upper mantle, related to the primordial magma ocean of the Moon, a result confirmed also by Gagnepain-Beyneix et al. (2004). Kuskov & Fabrichanaya (1994), Kuskov (1995), and Kuskov et al. (2002) confirmed that no mineralogical transformation can produce such an increase in the seismic velocities. These mineralogical interpretations of the seismic profiles are, however, not well adapted to the low-quality velocity models: Future steps are necessary with direct inversions of the seismic travel times and other geophysical data in terms of mineralogy (e.g., Verhoeven et al. 2004; A. Khan, J. Maclennan, S.R. Taylor, K. Mosegaard, J. Gagnepain-Beyneix, and P. Lognonné, submitted manuscript).

The Seismically Unknown Lower Mantle and Core

All Apollo seismic stations were located on the near side of the Moon, and no seismic signals associated with rays propagating through the core were detected (Figure 6, see color insert) with the exception of a single meteoroid impact (Nakamura et al. 1974). No events from within about 40 degrees of the center of the far side of the Moon have been identified by the most recent search (Nakamura 2004). Both studies suggest therefore that the very deep Moon mantle below the deep Moonquakes sources (at depth larger than 1000 km) strongly attenuates or deflects seismic waves; however, its seismic velocities remain unconstrained. The existence for a low velocity core presented by Nakamura et al. (1974) also needs to be confirmed, as already noted by Goins et al. (1981) and Sellers (1992).

Many studies do, however, support a small core (see Hood & Zuber 2000 for a review). Some arguments from geochemical analysis and mare basalt samples

indeed show a depletion of highly siderophile elements (e.g., Righter et al. 2000) but could be attributed to the formation of the proto-Moon core. Most geophysical arguments are stronger. Hood & Jones (1987) and Bills & Rubincam (1995) showed that a priori mantle density profiles cannot explain alone the mean density and inertia factor. A small core is strongly supported by these data, and explains also the induced magnetic dipole moment produced by the interaction of the Moon with Earth's geomagnetic tail, which requires a 340 $\pm$ 90 km conductive core (Hood et al. 1999). Finally, Williams et al. (2001) have shown that the rotation of the Moon was influenced by a dissipation source, interpreted as the signature of a liquid core.

A few researchers have searched in the Apollo seismic record of large events for low angular order free oscillations, which are very sensitive to the core structure. A first unsuccessful attempt was performed by Loudin & Alexander (1978). More recently, Khan & Mosegaard (2001) performed an inversion of the deep lunar structure with Apollo broadband data below 11 mHz, taking for the seismograms a summation of free oscillations. Both the frequencies and the amplitudes of the normal modes were inverted. The seismograms used by Khan & Mosegaard (2001) are indeed the strongest natural impacts of the profile shown in Figure 3. The seismic signals are however still weak and these impacts can be compared in magnitude to the impacts of the Saturn IVB (Figure 2). The mass and velocity give an impulse of 3.82×10^7 Ns, and an impulse 25 times larger (i.e., 10^9 Ns) will generate seismic waves saturating all Apollo seismometers in the 0.3–1 Hz frequency range (only 1024 DU of dynamic were available on the Apollo seismometers). This upper estimate of the impacts obtained by Khan & Mosegaard (2001) can be used to model the amplitude of seismograms for a spherical Moon model and with normal mode seismograms (Lognonné & Clévédé 2002). Figure 7*a* clearly shows that even in this upper case, the spectral amplitude of the signals are two orders of magnitude smaller than the instrument noise, greater than 10^{-9} $ms^{-2}/Hz^{1/2}$ at frequencies smaller than 10 mHz. If we furthermore consider that the three-dimensional structure and the scattering of the crust and upper mantle are reducing these amplitudes, and that a more precise analysis of these large events gives an upper limit of approximately 3×10^8 Ns (Lombardi et al. 2002), the signal-to-noise ratio achieved in the normal mode bandwidth (1–10 mHz) is smaller by two to three orders of magnitude than one for the Apollo data used by Khan & Mosegaard (2001).

The other candidates for such normal mode excitation are the HFT events with seismic moments up to 1.6×10^{15} Nm (Oberst 1987). A scaling of the amplitude of Figure 7*b*, computed for a shallow quake with moment of 10^{18} Nm shows amplitudes in the range of 10^{-10}–5×10^{-10} $ms^{-2}/Hz^{1/2}$ in the normal mode bandwidth. If such amplitudes are still too small for the Apollo seismometer noise, they could be detected with modern very broad band seismometers or superconducting gravimeters, if continuous operation during 5–10 years is possible (Gudkova & Zharkov 2002).

In the absence of normal modes and core phases, the density, moment of inertia, Love number k_2, and magnetic properties of the core are the only parameters able to constrain the core. They can however be jointly inverted with seismic constraints

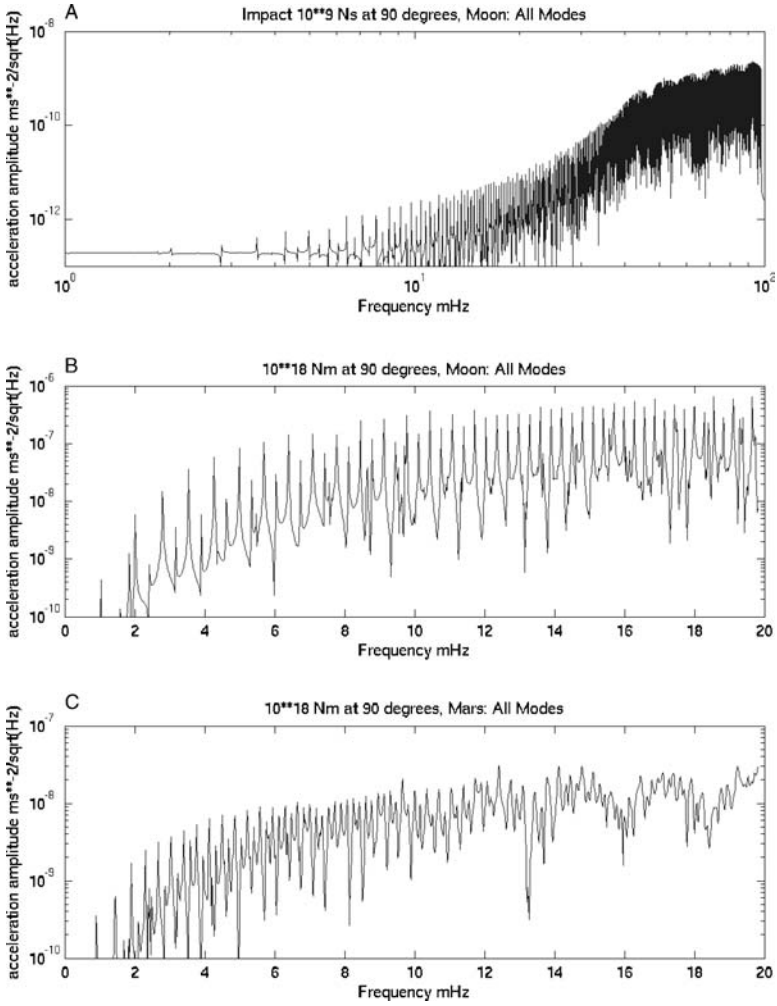

Figure 7 (*a*) Amplitude spectral density of a one-day seismic signal recorded on the vertical component at an epicentral distance of 90°. The source is an impact source with an impulse of 10^9 Ns. Below 10 mHz, the amplitudes are smaller than 2×10^{-12} ms^{-2}/Hz$^{1/2}$ and therefore at least 100 times smaller than the instrument noise at this frequency. (*b*) Spectral amplitude on the Moon for a 24-h record and at frequencies below 20 mHz for a synthetic quake releasing a moment of 10^{18} Nm at 30 km depth with strike, deep, and rake angles of 45°, 45°, and 45°, respectively. Such a quake is approximately three orders of magnitude greater than the strongest HFT quake. Azimuth is 20° and the epicentral distance is 90°. (*c*) Same synthetic quake, epicentral distance, and azimuth, but on Mars. At 5 mHz, the amplitudes exceed 1 ng/sqrt(Hz) and are a factor of four greater than those observed on Earth for an equivalent quake at equivalent epicentral distances. Note that below 10 mHz, most of the signal is in the fundamental modes.

on the mantle and crust. Such joint analysis was done first by Bills & Ferrari (1977) with the density, moment of inertia, and a preliminary seismic model and remains to be performed with the most recent seismic models. More recent estimates are from Kuskov & Kronrod (1998) and Kuskov et al. (2002) with the Nakamura (1983) seismic models and with the improved density and inertia factors. A pure γ-Fe core with density of 8100 kg/m^3 and a radius of 350 km or a core with smaller densities and larger radius, including the largest troilite FeS core with a radius of 530 km and a density of 4700 kg/m^3 were proposed. With the same inertia factor and mean density, but with their seismic model, Lognonné et al. (2003) have found densities in the range of 7000 kg/m^3 to 8000 kg/m^3 for a 350 km core, depending on the thickness of a 2910 kg/m^3 dense crust. These results can be compared to the latest results performed without seismic a priori data performed by Khan et al. (2004), for which a core with a radius of approximately 350 km and a density of 7200 kg/m^3 is found from the inversion of the density, moment of inertia, and of the real and imaginary parts of the Love number k_2.

MARS SEISMOLOGY

The past 15 years have been rather disappointing for Mars seismology. The early 1990s indeed started with great prospects for the seismic exploration of Mars, with the ambitious Soviet Mars94 mission with a very large orbiter, two small autonomous stations equipped with the short-period optimism seismometers (Lognonné et al. 1998a), and two penetrators. At the same time the assessment phase of the joint Mesur-Marsnet project (Solomon et al. 1991; Chicarro et al. 1991, 1993) started, with a goal of up to 12–16 seismic and meteorological stations from the U.S. Space Agency (NASA) in addition to the four stations of the European Space Agency (ESA). However, budgetary and programmatic problems in 1993 led to the postponement of the Mars94 mission to 1996, and the loss of the Mars Observer mission forced NASA to cancel Mesur. In 1996, hope returned with the last preparation for the Mars96 launch and with a new ESA-NASA InterMarsnet phase A, with a more reasonable network of four stations (Banerdt et al. 1996). But again, InterMarsnet did not make it through the ESA's selection process, and a few months later, after a successful launch, Mars96 failed its insertion into a trans-Mars trajectory and fell into the Pacific Ocean.

But the strikingly consistent "Phoenix" character of Network mission was ready for a rebirth in 1997 with the NetLander mission (see Sotin et al. 2000 and in the following papers a complete description of the payload of the mission). Despite two attempts for an ESA launch (on the MarsExpress mission or the possible F2/F3 MASTER mission), the European and U.S. Netlander team had to rely on the major collaboration between the United States and French space agencies for reaching Mars as a piggyback passenger of a Mars Sample Return orbiter. But again, programmatic and budgetary problems led to the project's collapse in 2003 during phase B of the mission (Butler 2003), two years after the cancellation of the sample return efforts.

Interior Structure of Mars

The interior of Mars remains, therefore, largely unconstrained, and only the four geophysical numbers (mean density, inertia factor, real, and imaginary k_2 value) are available in addition to the constraints put by Martian meteorites and by mineralogical or cosmochemical models. See Spohn et al. (1998) for a review on the Mars interior and Khan et al. (2004) for an inversion of these geophysical data.

Seismic models of Mars were, however, proposed by several authors already after the Viking mission. Okal & Anderson (1978) based their model on the Preliminary Reference Earth Model (PREM) of Dziewonski & Anderson (1981) and adjusted the core size to the sole mean density. Sohl & Spohn (1997) and Zharkov & Gudkova (2000) used an estimated value of the inertia factor ($C = 0.365\ Ma^2$ instead of the observed $C = 0.366 \pm 0.0018$) corrected for the nonhydrostatic contribution of the Tharsis bulge as well as geochemical constraints (Figure 8). The latter were based on the Dreibus & Wänke (1985) mixture models in which Mars is a mixture of 40% volatile rich and 60% volatile depleted C1 material constrained by the composition of the SNC meteoroids. But other mixtures models have been

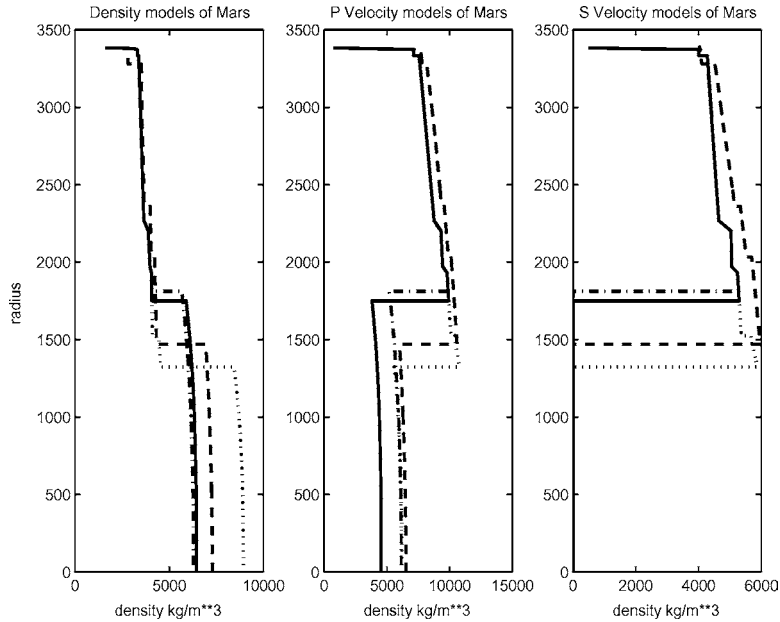

Figure 8 Models of Sohl & Spohn (1997) (*dashed line*) and three models of Gudkova & Zharkov (2004) (*solid, dashdotted, and dotted lines*). The solid line and dotted line are for a hydrogen content in the core of 50% (model M6) and 70% (model M7), respectively, with 14% sulfur in both cases, whereas the dashdotted line is for a sulfur content of 36% without hydrogen. The Sohl & Spohn (1997) model A has no hydrogen and 14% sulfur.

proposed to match the $\delta^{17}O/\delta^{18}O$ ratio between H and enstatite EH chondrites (Sanloup et al. 1999) or CI, CV, and H chondrites (Lodders & Fegley 1997).

However, these geochemical models generally do not agree with geophysical data, even for the mean density and inertia factors. The Sanloup et al. (1999) model, for example, provides an inertia factor of $C = 0.365\ Ma^2$, whereas the Dreibus & Wänke (1989) model gives $C = 0.357\ Ma^2$ (Sohl & Spohn 1997). Although this discrepancy might be related to the inadequacies of the geochemical models, Gudkova & Zharkov (2004) further considered light elements in the core, especially hydrogen, to decrease the density of the core and therefore to increase the inertia factor (i.e., by reducing the density contrast between mantle and core) while keeping the mass of the planet constant (i.e., by increasing the core size). If the chalcophile depletion of SNC indicates a sulfur rich core, very few constraints on the amount of hydrogen are indeed available, as well as for other light elements. Hydrogen was, however, available during the formation of the planet in enough amounts to build a pure FeH core. Other arguments support a large core with light elements. The first one is the newly determined value of tidal k_2 Love number of Mars [0.153 ± 0.017 (Yoder et al. 2003)]. Such a high value requires models with a large core radius, as shown by van Hoolst et al. (2003). Figure 9 shows that the best fit is achieved with those models with hydrogen, whereas those without hydrogen

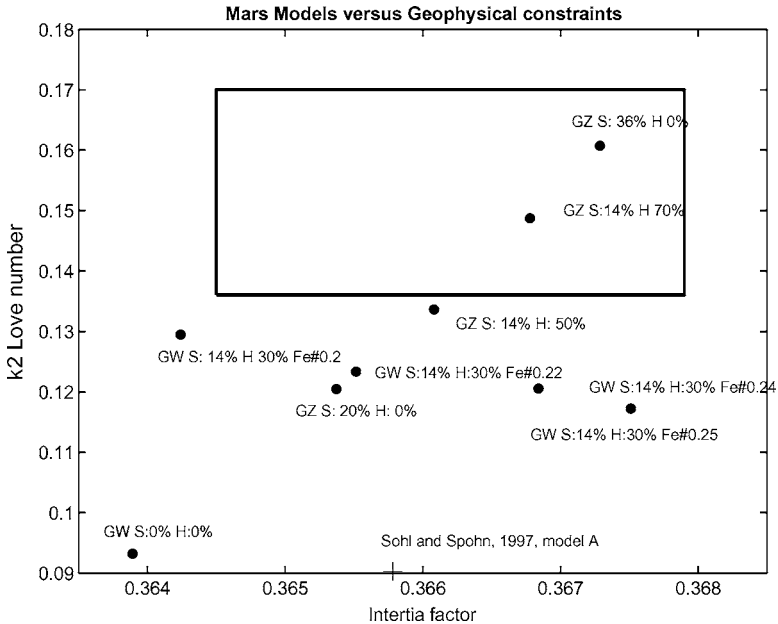

Figure 9 Fit of the observed and computer k_2 and inertia factors for the model A of Sohl & Spohn (1997) (+) and several models of Gudkova & Zharkov (2004) (o). Values within the box fit to the observed values within their error bars.

[Model M8 of Gudkova & Zharkov (2004) or model A of Sohl & Spohn (1997)] do not explain k_2. Although the core radius is 1468 km for model A, it is 200–300 km larger for the preferred models M6 and M7 (1662 km and 1753 km, respectively). Corresponding density at the core mantle boundary are 6936 kg m^{-3}, 6279 kg m^{-3}, and 5901 kg m^{-3}. The second is related to the a priori liquid state of the core. A liquid core is indeed supported by both the Phobos tidal acceleration value and by the large k_2 value. As noted by Lognonné & Mosser (1993) and Zharkov & Gudkova (1997), a low Martian Q at the Phobos tidal period will imply unrealistically low intrinsic Q of the planet if the core is solid and tidal stresses are distributed along the full solid planet. In contrast, Q corresponding to silicate material slightly colder than the Earth mantle is found for a liquid core (Lognonné & Mosser 1993). But as for Earth (Hillgren et al. 2000), hydrogen and sulfur are not the only candidates, and other elements could be advocated for a lighter density of a liquid core, especially silicium (Stevenson 2001, Sanloup et al. 2002), oxygen, or carbon. A low shear velocity zone at the base of the mantle could also impact the Love number value.

From a geochemical point of view, a large core increases the Fe/Si ratio to values closer to the 1.71 of the Martian meteorites. Indeed, the Fe/Si ratio for the two best models, M6 and M7, are 1.55 and 1.68, respectively, much larger than the 1.35 of model A from Sohl & Spohn (1997). But a larger core also has major consequences on internal structure and planetary evolution. One consequence is to make a perovskite-bearing lower mantle impossible owing to insufficient pressures in the present mantle. If such an endothermic phase transition from spinel to perovskite has been proposed as the driver of a one-plume convection pattern, resulting in the formation of the Tharsis bulge during the first billion of years (Harder & Christensen 1996), other explanations are however possible, such as an hemispheric dichotomy in the crustal insulation (Stegman et al. 2004). A determination of the core size and better constraints on the temperature of the core-mantle boundary will therefore allow researchers to determine if a geodynamical evolution of Mars with an initial hot mantle and such a discontinuity was ever possible and if the vanishing of this discontinuity with the mantle secular cooling might have influenced the planetary evolution.

Seismology therefore will be required to improve our knowledge of the Martian structure and our understanding of its evolution. Let us consider the different existing models proposed for the Mars mantle, shown in Figure 10, and address the possible differences in the different seismological observations. The simplest seismological secondary data that can be extracted from seismic data are the travel times of P and S waves, the group and phase velocities of surface waves (in the long-period range, 10 m–0.1 Hz), and the frequencies of the fundamental spheroidal modes. The latter two are shown in Figure 11, and differences of several tens of percents can be observed among these models. Such zero-order differences will be easily constrained as soon as seismic signals are successfully recorded. Therefore, I detail in the following section the a priori seismic signals, noise, and propagation properties on Mars and estimate the prospects of a future seismic experiment on this planet.

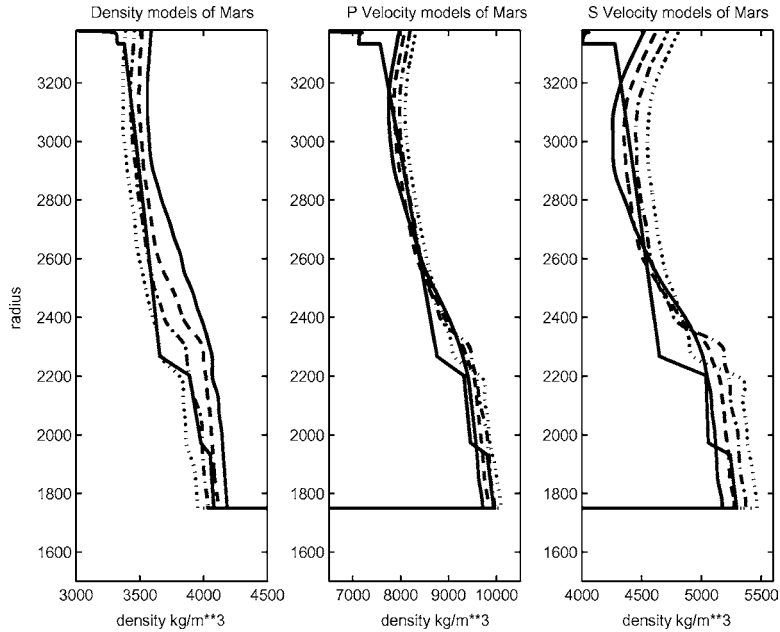

Figure 10 Mantle models of Mars in terms of density and seismic velocities for the model M7 of Gudkova & Zharkov (2004) (*continuous line*) and the four models of Mocquet et al. (1996). Models of Mocquet et al. (1996) have an increasing content of iron of 10%, 20%, 30%, and 40% represented by the dotted, dashdotted, dashed, and solid lines, respectively. The main effect of an increase in iron is to smooth the seismic discontinuities associated with α-olivine to β-spinel and β-spinel to γ-spinel. The Gudkova & Zharkov model has a 22% iron content in the mantle. The difference in depth of the discontinuities is mainly related to change in the core mantle boundary temperature. A temperature of approximately 2100 K is taken at the core mantle boundary for the model of Gudkova & Zharkov (2004), whereas a more complex model, with temperature inversion in the mantle and mantle temperature approximately 500 K colder at the depth of the discontinuities, is taken by Mocquet et al. (1996). These colder temperatures shift the discontinuity to a shallower depth.

Seismic Activity and Seismic Noise

A mission deploying a single or two very broad band (VBB) seismometers has never been successfully performed on Mars, leaving the seismic activity and seismic noise of the planet unknown. If wind-generated noises were indeed the main source of external noise during the Viking seismic experiment (Anderson et al. 1977), then such noise was clearly related to the vibrations of the lander in the wind (see Lognonné & Mosser 1993 for a detailed explanation). But during the windy periods, however, the seismometer was unable to resolve the local seismic

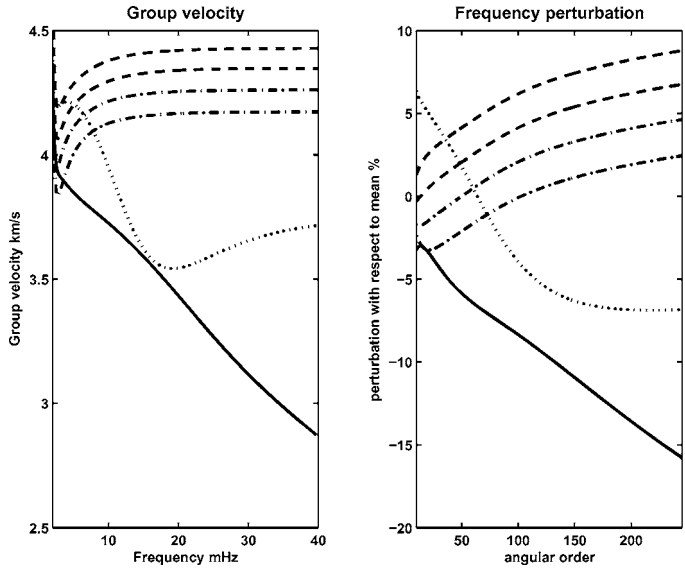

Figure 11 Primary long-period seismic observables for different Mars models. Left: the group velocities of Rayleigh waves with respect to frequency. Right: the fundamental spheroidal relative frequencies perturbations. The perturbations are computed for the mean values of all models listed. The dotted line is for model A of Sohl & Spohn (1997), the continuous line is for model M7 of Gudkova & Zharkov (2004), and the two dashed and two dashdotted lines are for the four models of Mocquet et al. (1996) with increasing content of iron from 10% to 40%. Note that the crustal structure is also different for all models.

noise, and we can therefore expect quite low noise levels (Nakamura & Anderson 1979), especially compared to Earth, where oceans are the major source of the so-called micro-seismic noise.

For the seismic activity, in addition to meteoroid impacts (Davis 1993), we expect natural quakes related to at least the thermoelastic cooling of the lithosphere. Estimates by Golombek et al. (1992) from surface fault observations and by Philipps et al. (1991) from a theoretical estimate of the thermo-elastic cooling of the lithosphere provide some idea of the seismic activity. It was found to be 100 times greater than the shallow Moonquake activity detected by the Apollo seismometers. But amplitudes of the largest Mars seismic signals will still be approximately four orders of magnitude (about 2.5 in M_s magnitude) lower than those of the largest earthquakes at long periods, i.e., at frequencies below the source cutoff of the largest quakes. More in detail, the Martian activity might provide about 50 quakes of seismic moment 10^{15} Nm per year, with an increase/decrease of the frequency by 5 for a decrease/increase of the seismic moment by 10, which represents a seismic activity releasing a moment of 10^{18}–10^{19} Nm per year. The distribution of this seismic activity has been studied in more

detail by Oberst et al. (2004). With a total of approximately 7000 faults with a cumulated length of 600,000 km found, they confirmed the higher seismic activity of Tharsis.

Martian noise has been estimated by Lognonné & Mosser (1993) for wind-generated noise, and by van Hoolst et al. (2003) for the temperature-generated noise. The typical estimate for the ground accelerations produced by the direct deformation of the Martian surface by the wind pressure fluctuation could have peak-to-peak amplitudes of the order of 10^{-9} ms^{-2} in the range of 0.1 to 0.01 Hz during relatively calm conditions, with wind speed of the order of 4 m/s (Lognonné & Mosser 1993). Moreover, Lognonné et al. (1996) have shown that even on Earth, seismometers can resolve such noise levels in quiet sites if protected by a light wind-shield. In contrast to the Viking case, the temperature variations might therefore be the major source of noise for surface-installed VBB seismometers. However, as shown by van Hoolst et al. (2003), most of the temperature variations on Mars are associated with the daily cycle and can be approximated by a Fourier series with the fundamental (of 24 h 56 min) and its harmonics. Moreover, thermal insulation of space-qualified seismometers can reach time constants of approximately 4 h and will reduce, therefore, the temperature variations by a factor of approximately 15 at 1 mHz, and approximately 150 at 10 mHz, leading to temperature fluctuations smaller than a fraction of a degree in the seismic band. An installation with a noise comparable to the Earth low noise model (e.g., approximately 10^{-9} $m/s^2/Hz^{1/2}$ in the seismic bandwidth) is therefore a realistic challenge, especially if an environmental correction performed through a recording of the pressure and temperature data is possible (e.g., Beauduin et al. 1996).

Normal Modes Excitation

Although the extraction of internal structure information with the direct body waves will need a precise localization of the events and therefore at least three stations for travel times analysis (six secondary data enabling the determination of the four source parameters and the two mean mantle velocities), surface waves, normal modes, and tidal analysis have the potential to provide useful information on the interior with fewer stations. For the sensitivity of normal modes to the Martian interior structure, see the series of papers by Okal & Anderson (1978), Lognonné et al. (1996), Gudkova & Zharkov (1996a,b). The perspectives developed here are important if the future missions deploy only one or two VBB seismometers on the Martian surface for long observation periods.

A Martian activity releasing a cumulated activity of 10^{18}–10^{19} Nm per year offers statistically the possibility to detect large quakes if the monitoring is performed during one or more Martian year. The excitation of normal modes by such quakes was studied by Lognonné et al. (1996) and later by Gudkova & Zharkov (2004), who both concluded that the observation of normal modes between 5 mHz and 20 mHz will be possible with a noise level of 10^{-9} $ms^{-2}/Hz^{1/2}$ by stacking methods on quakes with a cumulative 10^{18} Nm moment or by single record analysis of the

greatest quakes (Figure 7*c*). The observation of normal modes below 5 mHz will be more challenging with such quakes, and the search for continuous excitation of normal modes by the atmosphere is a possible alternative. Originally proposed by Kobayashi & Nishida (1998), the expected amplitudes are smaller by a factor of two to three than Earth values, and are therefore typically a fraction of nanogals (Lognonné et al. 2000, Tanimoto 2001). These early studies, however, have not fully taken the properties of the Martian atmosphere into account. They might also be considered with some caution, with the recent claims for an oceanic origin for Earth excitation of continuous oscillations (Rhie & Romanowicz 2004, Tanimoto 2005). Improved analysis, performed by Suda et al. (2002) by using Pathfinder data, have indeed obtained very low amplitude for the excitation, typically of the order of 3×10^{-10} ms^{-2}/Hz$^{1/2}$ for a correlation length of approximately 2 km for the atmospheric turbulences. Only correlation length of 10 km or more could lead to observable signals. Future works therefore will have to estimate the continuous and more coherent (on a large scale) excitation associated with the atmospheric global circulation winds and pressure using an explicit computation of the pressure glut (Lognonné et al. 1994) and with global circulation models. Even though the search for continuous excitation will be challenging due to the low level of excitations, it might open exciting perspectives for the detection of the lowest angular order normal modes and must be taken into account for the specification of instruments' noise levels.

Surface Waves

At higher frequencies and in the band 5 mHz–50 mHz, surface wave analysis can also be performed for the large quakes, including in the limited case of a two-station network equipped with three axis seismometers and therefore able to determine the back-azimuth of surface waves. The simple model shows that relative errors in the epicentral distance of less than 2.5% can be achieved over a wide equatorial band of the planet ($\pm 20^\circ$ latitude) for two typical landing sites around the Tharsis bulge when back-azimuth errors of 15° are assumed. Such measurements could constrain the major differences of the already proposed models of the mantle but they will be limited by the sensitivity of surface waves azimuth with respect to lateral variations and therefore unable to get the precision necessary to resolve smaller differences, such as those related to the FeO content in the mantle (Mocquet et al. 1996). On Earth, back-azimuth perturbations related to asphericity indeed can reach typically 10°, and very likely, the relatively larger crustal variations on Mars will lead to larger effects (Larmat et al. 2002). However, as observed on Earth, a large part of the lateral variations of surface waves can be modeled with a priori on the lithosphere and upper mantle (Nataf & Ricard 1996). With the increasing constraints on the crustal and lithosphere thickness (e.g., Zuber 2001, Wieczorek & Zuber 2004), we can expect future developments for the simulation of surface waves in complex three-dimensional crustal models of Mars.

Detection of Body Waves

Large differences in the travel times of body waves exist between the models proposed by Gudkova & Zharkov (2004), Sohl & Spohn (1997), and Mocquet et al. (1996). For P waves, they can reach approximately 10 s for epicentral distances up to 40° and can be a few tens of seconds for larger distances. Being excited by relatively low magnitude quakes, body waves will therefore be, as in the case of the Moon, the primary source of information on the deep interior. The main limitation for the detection of body waves on Mars is related to attenuation and to the scattering in the crust owing to the impacting history, especially in the southern hemisphere highlands. The importance of attenuation on Mars was originally pointed out by Goins & Lazarewicz (1979), who have shown that the Viking seismometer with a 4 Hz central frequency was unable to detect remote events owing to attenuation. Low Q factors of the Martian mantle are indeed supported by the high secular acceleration of Phobos, which is explained by a shear quality factor of approximately 100 at the tidal period of Phobos and of approximately 200 in the seismic band (Lognonné & Mosser 1993, Zharkov & Gudkova 1997) for liquid core models. These values can be compared to Earth, where body waves are mainly attenuated in Earth's upper mantle due to shear attenuation ($Q_{shear} = 150$) and encounter a smaller attenuation in the lower mantle ($Q_{shear} = 300$, Dziewonski & Anderson 1981). In the upper mantle and for 5 km/s S waves, this gives a reduction of amplitude by 10 after approximately 550 km of propagation at 1 Hz, and only 137 km at 4 Hz. More specifically, the amplitudes of body waves on Mars are plotted by Figure 12*a*,*b* (after Mocquet 1998). The amplitudes are computed for two frequency bands (0.1–1 Hz and 0.5–2.5 Hz) and for a near-surface and isotropic source with a seismic moment of 10^{15} Nm. The crustal transmission is taken into account, as well as the geometrical spreading and attenuation for a Mars model compatible with the present a priori knowledge.

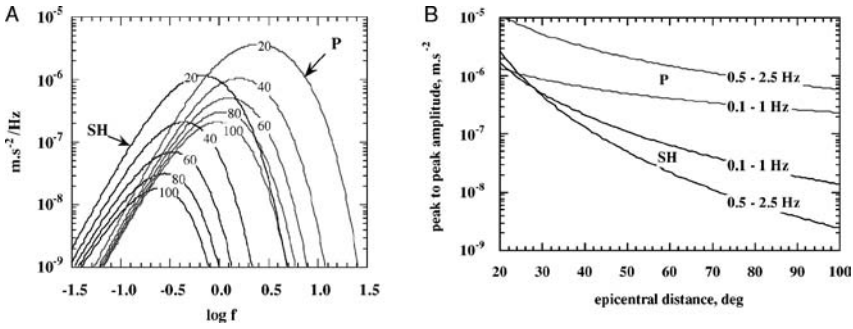

Figure 12 (*a*) Fourier transformed amplitude of the P and S body wave packet. The amplitude is plotted with respect to frequency for different epicentral distances. (*b*) Maximum peak-to-peak amplitude in the frequency band with respect to epicentral distance. Figures after Mocquet 1998 for a quake with a seismic moment of 10^{15} Nm.

The amplitudes at frequencies higher than 0.5 Hz (0.5–2.5 Hz) decrease strongly with epicentral distance. P waves in the frequency band 0.1–1 Hz are less sensitive. This frequency bandwidth was chosen for the Optimism seismometer onboard the lost Mars96 mission (with a 1 ng resolution in that bandwidth). At higher frequencies (0.5–2.5 Hz bandwidth), however, amplitudes decrease rapidly with the distance, and for S waves are even below the longer period amplitudes. Moreover, scattering could be strong at such frequencies. For shallow quakes it will reduce the amplitude of the P waves during the downward propagation from the crust to the mantle, near the source, and a second time during the upward propagation from the mantle to the surface near the receiver. The effect can lead to a reduction by 10 of the P wave energy and more for the amplitudes owing to the length of the coda. Body waves below a frequency of 1 Hz are therefore best adapted to the detection of Marsquakes. Assuming total detection for signals with accelerations greater than 10^{-8} m s^{-2} peak-to-peak, Mocquet (1998) has shown that 60% of quakes with seismic moments greater than 10^{14} Nm, i.e., corresponding to Earth magnitude greater than 3.2, can be detected by a four-station network. This might provide approximately 100 detected quakes out of the 140 quakes that are expected in one Martian year of Network operation.

INSTRUMENTATION AND PLANNED MISSIONS

We focus here on the missions and instruments under development. For a review on the planetary seismometers developed before 1990, see Lognonné & Mosser (1993). Since 1990, the development of new seismometers has been done mainly for the Moon, with the Lunar A two-axis seismometer (Mizutani et al. 1995, 2003), and for Mars, with the Mars96 Optimism vertical axis seismometer (Lognonné et al. 1996) and with the Mars Ultra-broadband seismic package (Lognonné et al. 1996) developed for future network missions. The latter is based on a two-axis VBB seismometer (Lognonné et al. 2000) and on a three-axis short-period microseismometer (Banerdt & Pike 2001), and can be adapted to a Lunar mission by a change of the spring. Table 2 provides the main characteristics and performances of the seismic instruments, whereas Figures 13*a–d* show the sensors heads and associated pendulum. The main difficulties in the construction of space-qualified seismometers, especially for broadband instruments, are related to the constraints in mass, shock/g-load (typically 200 g for a semi-hard lander and 1000–10000 g for a penetrator), and power allocation (<500 mW). For Mars, seismometers must in addition be protected against the fluctuation in the atmospheric pressure, the large daily temperature variations, and even local magnetic fields. Although a mass of approximately 2 kg for a complete broadband instrument (sensors, thermal protection, installation, leveling, acquisition, and command systems) is small compared to the Apollo instruments (11.5 kg; Latham et al. 1969) or to Earth instruments (13 kg for a STS2 without data logger and cables), it is

TABLE 2 Main performances and characteristics of the different developed or in-development seismometers

	Lunar A	**Optimism**	**VBB-SEIS**	**SP-SEIS**
Number of sensors and free period	One vertical, one horizontal, 1–1.2 Hz	One vertical 2 Hz	Two oblique axis 0.5 Hz	Three oblique axis 10 Hz
Complete mass	3500 g	840 g	2000 g	
Ground displacement resolution at 1 Hz and 5 Hz	1.25×10^{-10} m 0.20×10^{-10} m (5 Hz)	5×10^{-10} m	$<0.125 \times 10^{-10}$ m	$<1.25 \times 10^{-10}$ m $<0.05 \times 10^{-10}$ m (5 Hz)
Bandwidth (Hz)	0.8–10	0.2–2	0.003–10	0.02–50
Maximum sampling rate and dynamic	16 sps, 12 bits	4 sps, 16 bits	20 sps, 24 bits	100 sps, 24 bits
Consumption	175 mW	67,5 mW	450 mW	
g-load	10000 g	200 g–20 ms	200 g–20 ms	100 g–20 ms

The sensor mass is the mass of the pendulum, whereas the complete mass is for all the instrument, including its installation mechanism (when available, as for the VBB-SP SEIS package), control and acquisition electronics and hardness.

Bandwidth is defined as the frequency domain where the resolution is greater than 1/10 of the peaked resolution.

a significant fraction of the overall payload of a planetary lander, typically 6 kg for Network oriented landers. These mass constraints are particularly strong for LP instruments for which large mechanical amplification as well as a low thermal sensitivity (and therefore a large thermal inertia and protection in addition to thermal compensation) are needed. For details on the technical solutions see Mizutani et al. (2003), Lognonné et al. (1996), Banerdt & Pike (2001), and Lognonné et al. (2000).

Lunar A (Mizutani et al. 1995, 2003), the only remaining planetary seismology mission in development, will be launched probably in 2005–2006 after several delays. It will deploy two penetrators equipped with two axis seismometers. Its main goal will be the determination of the size of the lunar core. The first landing site will be close to the *Apollo 12* site, whereas the other will be at the antipode. Seismic signals will be detected by a long-term/short-term average detection algorithm and will be stored in the penetrator's memory for telemetry through the Lunar A orbiter during one year. The size of the core will be characterized through its focusing effect on body waves. However, owing to the continuous activity of the deep Moonquake, these two penetrators, as well as any future lunar seismic package, will be able to be operated in a virtual Apollo/post-Apollo network. Indeed, the deep Moonquake sources, already detected by the Apollo seismic stations, are probably still active. For each deep Moonquake, the Apollo stations will indeed provide eight arrival times, whereas the two penetrators will add four

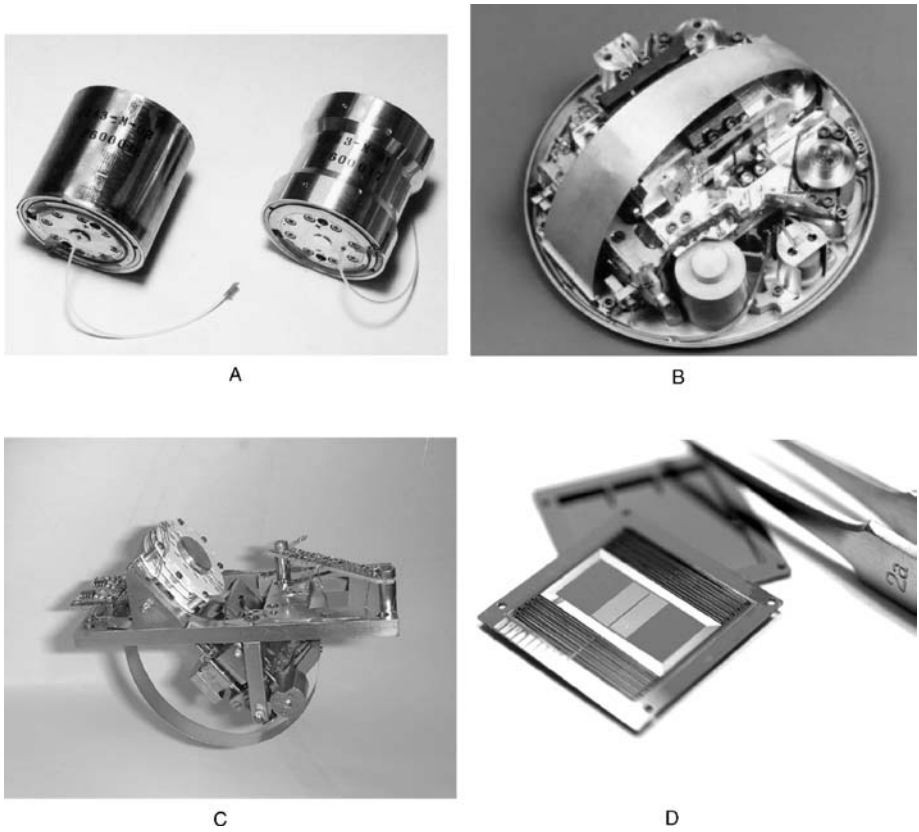

Figure 13 (*a*) Lunar A vertical and horizontal sensor head. The diameter is 5 cm and the mass is 354 g. (*b*) Optimism sensor head. Diameter is 8 cm and mass is 120 g. (*c*) VBB-SEIS sensor head (177.2 g). (*d*) SP suspension (mass is 35 g per axis). Mass is for the pendulum, the velocity or displacement transducers, and feedback coils and their mounting structure.

new arrival times to the data set associated to this given deep Moonquake. After estimation of the position and of the two source times, this will almost double the amount of data available for internal structure studies from four (8–4) to seven (12–5).

SUMMARY AND POSSIBLE FUTURE MISSIONS

The summary below is given for the Moon and Mars. In addition, brief information on proposed seismic missions to new planets (Venus, Europa, and small bodies) is given.

Moon

The Apollo Seismic Network was unable to determine the deep interior of the Moon and the size of the core and did not provide detailed models of the crust and Moon mantle. Stable velocities are found mainly for the upper mantle, and recent estimations of the crustal thickness (35–45 km) differ from previous ones (60–70 km). Although all models show a pyroxenite upper mantle, a more primordial lower mantle is tentatively proposed, with higher Mg numbers. The Japanese Lunar A mission, expected to launch before 2006, will therefore constrain the size of the core by direct seismic observations and will also greatly improve the velocity models of the deep mantle. The next step will be a network of VBB seismometers on the Moon (Neal et al. 2004) for future high-resolution seismic exploration of the Lunar three-dimensional internal structure with possibly six to eight landers.

Mars

The internal structure of Mars will remain unconstrained before the deployment of seismometers by future missions (Lognonné et al. 2003). Scientific objectives have been identified for single-station pathfinder observation (Banerdt & Lognonné 2003, Lognonné & Banerdt 2003), for two stations performing subsurface cryolithosphere exploration (Grimm 2002), and for a network mission such as the Netlander mission (Lognonné et al. 2000, Dehant et al. 2004). A seismic mission to Mars is therefore crucial to our understanding of the internal structure of the planet and must be proposed for the future mission opportunities to Mars.

Jovian and Saturnian Satellites

The exploration of the outer planets has revealed the complexity of the internal structure of the giant planets' satellites. See Kuskov & Kronrod (2001) and Sohl et al. (2002) for a recent review on their interior. Of special interest for future seismic studies will be the Jovian satellite Europa (e.g., Carr et al. 1998) and the Saturnian satellite Titan (e.g., Grasset et al. 2000, Sohl et al. 2003), in both of which the existence of an ocean covered by a icy crust is probable. Kovach & Chyba (2001) and Lee et al. (2003) have studied in detail the possibilities of seismic exploration of Europa. They have shown that a passive seismic experiment will be able to detect natural sources, either related to ice cracking, to tidal induced quakes, or to natural impacts, and that the recording of ice-shell trapped surface waves in the frequency band 0.1–10 Hz will allow the determination of the thickness of the solid ice crust.

Venus

Some estimation of the seismic activity, done for the past NASA Venus Internal Structure Mission study (Stofan et al. 1993), suggested a seismically active

planet. With a seismogenic layer of 30 km, more than 100 quakes of surface wave magnitude greater than 5, and approximately 25 quakes greater than 6, could be released by an intraplate activity with a strain rate of 10^{-19} s^{-1}. Instead of deploying a seismic network designed to survive the surface temperature of the planet (500°C), Lognonné et al. (2003) proposed to use the coupling between the solid planet and its atmosphere. As shown by Lognonné et al. (1998b), a significant coupling is found on Earth and has been used for the detection of seismic waves in the ionosphere (Ducic et al. 2003, Artru et al. 2004). On Venus, the coupling will be stronger owing to the better acoustic adaptation of the atmosphere with respect to the interior. The surface pressure (90 bars), density (60 kg/m^3) and acoustic velocities (410 m/s) provide a ground impedance approximately 60 times greater than on Earth. Moreover, an additional amplification is achieved by the propagation of the wave from the surface to the 1 bar level, resulting in effects approximately 500 larger than on Earth, where the wave reaches altitudes with similar densities. ESA's Venus Express mission, expected to launch in 2005, will therefore search, with its VIRTIS instrument, for atmospheric temperature anomalies related to the release of seismic energy (Marinangeli et al. 2004).

Small Bodies

Active seismology (with explosive or impactors) or passive seismology (with natural impacts) has been proposed several times for the exploration of the interior of asteroids (e.g., Walker & Huebner 2004) or for an optimization of deflection strategies in asteroid mitigation (Ball et al. 2004). As noted in the Introduction above, a first unsuccessful attempt was performed with the two SP seismometers onboard the Phobos landers (Surkov 1989). Asteroids, owing to their limited size and low gravity are strongly influenced by seismic waves: Free oscillations are typically observed between 0.1 and 10 Hz (Ball et al. 2004) and minor impacts on a asteroid may produce ground accelerations higher than the local gravity: seismic reverberation has therefore a major impact in the morphology of the asteroid regolith, including in the shape and density of small craters (Richardson et al. 2004). We therefore can expect that future missions toward asteroids will seriously consider the inclusion of seismic experiments in their payload.

ACKNOWLEDGMENTS

I would like to thank B. Banerdt, H. Mizutani, W. Pike, T. Spohn, C. Sotin, D. Giardini, B. Romanowicz, J.P. Montagner, and V. Dehant for their active support in planetary seismology and for constructive discussions during the past years, as well as the SEIS scientific and technical team. This work was partially supported by CNES, PNP, and IUF grants. I thank J. Gagnepain-Beineix for fruitful discussions, Y. Nakamura and A. Khan for constructive reviews, as well as an anonymous reviewer. Many recent papers reviewed here, as well as this review, were supported by the EC MAGE Training Network under contract RTN2- 2001-00,414, MAGE. This is IPGP contribution 2023.

The *Annual Review of Earth and Planetary Science* is online at http://earth.annualreviews.org

LITERATURE CITED

Anderson DL, Miller WF, Latham GV, Nakamura Y, Toksoz MN, et al. 1977. Seismology on Mars. *J. Geophys. Res.* 82:4524–46

Artru J, Farges T, Lognonné P. 2004. Acoustic waves generated from seismic surface waves: propagation properties determined from Doppler sounding observation and normal-modes modeling. *Geophys. J. Int*. 158:1067–77

Ball AJ, Lognonné P, Seiferlin K, Pätzold M, Spohn T. 2004. Lander and penetrator science for NEO mitigation studies. In *Mitigation of Hazardous Impacts Due to Asteroids and Comets*, ed. MJS Belton, DKYeomans, TH Morgan, 266:291. Cambridge, UK: Cambridge Univ. Press

Banerdt B, Chicarro AF, Coradini M, Federico F, Greeley R, et al. 1996. InterMarsnet, Phase A study report. *ESA Publ.* SCI(96)2

Banerdt WB, Lognonné P. 2003. An autonomous instrument package for providing "Pathfinder" network measurements on the surface of Mars. *Int. Conf. Mars, 6th, Pasadena, July 20–25, 2003,* Abstr. No. 3221. Houston, TX: Lunar Planet. Inst.

Banerdt WB, Pike WT. 2001. A miniaturized seismometer for subsurface probing on Mars. *Conf. Geophys. Detect. Subsurf. Water Mars, Houston, August 6–10, 2001*, Abstr. No. 7056. Houston, TX: Lunar Planet. Inst.

Beauduin R, Lognonné P, Montagner JP, Cacho S, Karczewski JF, Morand M. 1996. The effect of the atmospheric pressure changes on seismic signals or how to improve the quality of a station. *Bull. Seism. Soc. Am.* 86:1760–69

Bills BG, Ferrari AJ. 1977. A lunar density consistent with topographic, gravitational, librational and seismic data. *J. Geophys. Res*. 82:1306–14

Bills BG, Rubincam DP. 1995. Constraints on density models from radial moments: applications to Earth, Moon, and Mars. *J. Geophys. Res*. 100:26305–16

Buck WR, Toksoz MN. 1980. The bulk composition of the Moon based on geophysical constraints. *Proc. Lunar Planet. Sci. Conf., 11th*, 3:2043–58. Houston, TX: Lunar Planet. Inst.

Butler C. 2003. France purges space programme in bid to survive budget crisis. *Nature* 423:103

Canup RM, Righter K, eds. 2000. *Origin of the Earth and Moon*. Tucson: Univ. Ariz. Press

Carr MH, Belton MJS, Chapman CR, Davies ME, Geissler P, et al. 1998. Evidence for a subsurface ocean on Europa. *Nature* 391:363

Chenet H. 2003. *Etude de la structure interne de la Lune*. PhD thesis. IPGP Univ. Paris Denis Diderot. http://tel.ccsd.cnrs.fr/documents/archives0/00/00/58/39/index_fr.html

Chenet H, Lognonné P, Wieczorek MA, Mizutani H. 2004. A first crustal thickness map of the Moon with Apollo seismic data. *Lunar Planet. Sci. Conf., 35th*, Abstr. 1581. Houston, TX: Lunar Planet. Inst.

Cheng CH, Toksöz MN. 1978. Tidal stresses in the Moon. *J. Geophys. Res.* 83:854–53

Chicarro AF, Coradini M, Fulchignoni M, Hiller K, Knudsen JM, et al. 1993. Marsnet, phase A study report. *ESA Publ*. SCI(93)2

Chicarro AF, Coradini M, Fulchignoni M, Liede I, Lognonné P, et al. 1991. Marsnet, assessment study report. *ESA Publ*. SCI(91)6

Cooper MR, Kovach RL, Watkins JS. 1974. Lunar near surface structure. *Rev. Geophys. Space Phys*. 12:291–308

Dainty AM, Toksöz MN, Anderson KR, Pines PJ, Nakamura Y, Latham G. 1974. Seismic scattering and shallow structure of the Moon in Oceanus Procellarum. *Moon* 9:11–29

Davis PM. 1993. Meteoroid impacts as seismic sources on Mars. *Icarus* 105:469–78

Dehant V, Lognonné P, Sotin C. 2004. Netlander: a European mission to study the planet Mars. *Planet. Space Sci.* 52:977–85

Dreibus G, Wanke H. 1985. A volatile-rich planet. *Meteoritics* 20:367–82

Ducic V, Artru J, Lognonné P. 2003. Ionospheric remote sensing of the Denali Earthquake Rayleigh surface waves. *Geophys. Res. Lett.* doi:10.1029/2003GL017812

Duennebier F, Sutton GH. 1974. Thermal Moonquakes. *J. Geophys. Res*. 79:4351–64

Dziewonski AM, Anderson DL. 1981. Preliminary reference Earth model. *Phys. Earth Planet. Int*. 25:297–356

Gagnepain-Beyneix J, Gabsi T, Dayre P, Lognonné P. 2002. Apollo seismic data in mini-seed. http://ganymede.ipgp.jussieu.fr/GB/donnees/

Goins NR, Dainty AM, Toksöz MN. 1981a. Seismic energy release of the Moon. *J. Geophys. Res.* 86:378–88

Goins NR, Dainty AM, Toksöz N. 1981b. Structure of the lunar highlands site Apollo 16. *Geophys. Res. Lett*. 8:29–32

Goins NR, Dainty AM, Toksöz MN. 1981c. Lunar seismology: the internal structure of the Moon. *J. Geophys. Res.* 86:5061–74

Goins NR, Lazarewicz AR. 1979. Martian seismicity. *Geophys. Res. Lett*. 6:368–70

Golombek MP, Banerdt WB, Tanaka KL, Tralli DM. 1992. A prediction of Mars seismicity from surface faulting. *Science* 258:979–81

Grasset O, Sotin C, Deschamps F. 2000. On the internal structure and dynamics of Titan. *Planet. Space Sci.* 48:617–36

Grimm RE. 2002. The Naiades: A Mars scout proposal for electromagnetic and seismic groundwater exploration. Presented at *Am. Geophys. Union, Fall Meet.*, 2002, Abstr. #P12A-0368, San Fransisco

Gudkova TV, Zharkov VN. 1996a. The exploration of Martian interiors using the spheroidal oscillation method. *Planet. Space Sci.* 44:1223–30

Gudkova TV, Zharkov VN. 1996b. On investigation of Martian crust structure using the free oscillation method. *Planet. Space Sci.* 44:1231–36

Gudkova TV, Zharkov VN. 2002. The exploration of the lunar interior using torsional oscillations. *Planet. Space Sci.* 50:1037–48

Gudkova TV, Zharkov VN. 2004. Mars: interior structure and excitation of free oscillations. *Phys. Earth Planet. Int.* 142:1–22

Harder H, Christensen UR.1996. A one plume model of martian mantle convection. *Nature* 380:507–9

Hartmann WK, Philllips RJ, Taylor GJ, eds. 1984. *Origin of the Moon*. Houston, TX: Lunar Planet. Inst.

Hillgren VJ, Gessmann CK, Li J. 2000. An experimental perspective on the light element in Earth's core. See Canup & Righter 2000, pp. 245–64

Hood LL. 1986. Geophysical constraints on the lunar interior. See Hartmann et al. 1984, pp. 361–410

Hood LL, Jones JH. 1987. Geophysical constraints on lunar bulk composition and structure: a reassessment. *J. Geophys. Res*. 92: E396–410

Hood LL, Mitchell DL, Lin RP, Acuna MH, Binder AB. 1999. Initial measurements of the lunar induced magnetic dipole moment using Lunar Prospector magnetometer data. *Geophys. Res. Lett*. 26:2327–30

Hood LL, Zuber MT. 2000. Recent refinements in geophysical constraints on lunar origin and evolution. See Canup & Righter 2000, pp. 397–409

Horvath P, Latham GV, Nakamura Y, Dorman HJ. 1980. Lunar near surface shear wave velocities at the Apollo landing sites as inferred from spectral amplitude ratios. *J. Geophys. Res.* 85:6572–78

Khan A, Mosegaard K. 2001. New information on the deep lunar interior from an inversion of lunar free oscillation periods, *Geophys. Res. Lett*. 28:1791–94

Khan A, Mosegaard K. 2002. An inquiry into the lunar interior—A non-linear inversion of the Apollo seismic data. *J. Geophy. Res.* 107:doi: 10.1029/2001JE001658

Khan AK, Mosegaard, Rasmussen KL. 2000. A new seismic velocity model for the Moon from a Monte Carlo inversion of the Apollo

lunar seismic data. *Geophys. Res. Lett.* 27: 1591–94

Khan A, Mosegaard K, Williams JG, Lognonné P. 2004. Does the Moon possess a molten core? Probing the deep lunar interior using results from LLR and lunar prospector. *J. Geophys. Res*. 109:E09007, doi:10.1029/2004JE002294

Khan A, Mosegaard K, Lognonne P, Wieczorek M. 2004. A look at the interior of Mars. *Lunar Planet. Sci. Conf, 35th*, Abstr. No. 1631. League City, TX: Lunar Planet. Inst.

Kobayashi N, Nishida K. 1998. Atmospheric excitation of planetary free oscillations. *J. Physics: Cond. Matter* 10:11557–60

Kovach RL, Chyba CF. 2001. Seismic detectability of a subsurface ocean on Europa. *Icarus* 150:279–87

Koyama J, Nakamura Y. 1979. Re-examination of the lunar seismic velocity structure based on the complete data set. *Lunar Planet. Sci. Conf., 10th*, pp. 685–87. Houston, TX: Lunar Planet. Inst.

Kuskov OL. 1995. Constitution of the Moon: 3. Composition of middle mantle from seismic data. *Phys. Earth Planet. Int*. 90:55–74

Kuskov OL. 1997. Composition of the Moon: 4. Composition of the mantle from seismic data. *Phys. Earth Planet. Int.* 102:239–57

Kuskov OL, Fabrichnaya OB. 1994. Constitution of the Moon: 2. Composition and seismic properties of the lower mantle. *Phys. Earth Planet. Int.* 83:197–216

Kuskov OL, Kronrod VA. 1998. Constitution of the Moon: 5. Constraints on composition, density, temperature and radius of a core. *Phys. Earth. Planet. Int*. 107:285–306

Kuskov OL, Kronrod VA. 2001. Core sizes and internal structure of Earth's and Jupiter's satellites. *Icarus* 151:204–27

Kuskov OL, Kronrod VA, Hood LL. 2002. Geochemical constraints on the seismic properties of the lunar mantle. *Phys. Earth. Planet. Int*. 134:175–89

Lammlein D. 1977. Lunar seismicity and tectonics. *Phys. Earth Planet. Int.* 14:224–73

Lammlein D, Latham GV, Dorman J, Nakamura Y, Ewing M. 1974. Lunar seismicity, structure and tectonics. *Rev. Geophys. Space Phys*. 12:1–21

Larmat CS, Capdeville Y, Montagner J, Banerdt B, Lognonné P, Vilotte J. 2002. Simulation of the effect of topography and crustal thickness on the Martian seismograms by the coupled method. *Am. Geophys. Union Fall Meet.,* Abstr. #P62A-0367, San Francisco

Larson EWF, Ekström G. 2002. Determining surface wave arrival angle anomalies. *J. Geophys. Res*. 107:doi:10.1029/2000JB000048

Latham G, Ewing M, Press F, Sutton G. 1969. The Apollo passive seismic experiment. *Science* 165:241–50

Latham GV, Ewing M, Dorman J, Press F, Toksöz N, et al. 1970. Seismic data from man-made impacts on the Moon. *Science* 170:620–26

Latham GV, Ewing M, Dorman J, Lammlein D, Press F, et al. 1971. Moonquakes. *Science* 174:687–92

Lee S, Zanolin M, Thode AM, Pappalardo RT, Makris NC. 2003. Probing Europa's interior with natural sound sources. *Icarus* 165:144–67

Lehner FE, Witt EO, Miller WF, Gurney RD. 1962. A seismometer for lunar experiments. *J. Geophys. Res*. 67:4779–86

Linkin V, Harri AM, Lipatov A, Belostotskaja K, Derbunovich B, et al. 1998. A sophisticated lander for scientific exploration of Mars: Scientific objectives and implementation of the Mars96 Small Station. *Planet. Space Sci.* 46:717–37

Lodders K, Fegley B. 1997. An oxygen isotope model for the composition of Mars. *Icarus* 126:373–94

Lognonné P, Banerdt WB. 2003. Rationale for seismic measurements on Mars by a single station. *Int. Conf. Mars, 6th, Pasadena*, Abstr. No. 3225. Houston, TX: Lunar Planet. Inst.

Lognonné P, Clévédé E. 2002. Chapter 10: Normal modes of the Earth and planets. In *Handbook on Earthquake and Engineering Seismology*, IASPEI Centen. Publ., Int. Geophys. Ser. 81A, ed. H Kanamori, P Jennings, W Lee. San Diego, CA: Academic Press

Lognonné P, Zharkov VN, Karczewski JF, Romanowicz B, Menvielle M, et al. 1998a. The seismic optimism experiment. *Planet. Space Sci.* 46:739–47

Lognonné P, Clévédé C, Kanamori H. 1998b. Normal mode summation of seismograms and barograms in an spherical Earth with realistic atmosphere. *Geophys. J. Int*. 135:388–406

Lognonné P, Gagnepain-Beyneix J, Banerdt WB, Cacho S, Karczewski JF, Morand M. 1996. An ultra-broad band seismometer on InterMarsnet. *Planet. Space Sci.* 44:1237–49

Lognonné P, Gagnepain-Beyneix J, Chenet H. 2003a. A new seismic model of the Moon: implication in terms of structure, formation and evolution. *Earth Planet. Sci. Lett.* 6637:1–18

Lognonné P, Garcia R, Romanowicz B, Banerdt B. 2003b. A new concept for seismology on Venus using orbiting radar instead of landers. *Am. Geophys. Union Fall Meet.* Abstr., San Francisco

Lognonné P, Giardini D, Banerdt B, Gagnepain-Beyneix J, Mocquet A, et al. 2000. The NetLander very broad band seismometer. *Planet. Space Sci*. 48:1289–302

Lognonné P, Mosser B. 1993. Planetary seismology. *Surv. Geophys.* 14:239–302

Lognonné P, Mosser B, Dahlen FA. 1994. Excitation of the Jovian seismic waves by the Shoemaker-Levy 9 cometary impact. *Icarus* 110:186–95

Lognonné P, Spohn T, Giardini D. 2003c. Mars in depth. *Astron. Astrophys.* 44:15

Lognonné P, Gagnepain-Beyneix J, Chenet H, Spohn T. 2004. Constraints on the temperature and mineralogy of the Moon from a joint inversion of Apollo seismic, geodetic data and LP-clementine gravity data. Presented at Am. Geophys. Union, Fall Meet., 2004, Abstr. #G43A-0803, San Francisco

Lombardi D, Lognonné P, Gagnepain-Beyneix J, Gudkova T. 2002. Calibration des impacts naturels et artificiels sur la Lune ou Mercure. *Colloq. Programme Natl. Planétol*., *Nantes*, pp. 58–59

Loudin MG, Alexander SS. 1978. Observed estimates of spheroidal free oscillations of the Moon and their interpretation. *EOS Trans. Am. Geophys. Union* 59:1124

Marinangeli LL, Baines K, Garcia R, Drossart P, Piccioni G, et al. 2004. Venus surface investigation using VIRTIS onboard the ESA/Venus express mission. *Lunar Planetary Sci. Conf., 35th, League City, TX*, Abstr. No. 1363

Mark N, Sutton GH. 1975. Lunar shear velocity structure at Apollo sites 12, 14, and 15. *J. Geophys. Res*. 80:4932–38

Mizutani H. 1995. Lunar interior exploration by Japanese lunar penetrator mission, Lunar-A. *J. Phys. Earth* 43:657–70

Mizutani H, Fujimura A, Tanaka S, Shiraishi H, Nakajima T. 2003. Lunar-A mission: goals and status. *Adv. Space Res.* 31:2315–21

Mocquet A. 1998. A search for the minimum number of stations needed for seismic networking on Mars. 1999. *Planet. Space Sci.* 47:397–409

Mocquet A, Vacher P, Grasset O, Sotin C. 1996. Theoretical seismic models of Mars: the importance of the iron content of the mantle. *Planet. Space Sci.* 44:1251–68

Mueller S, Taylor GJ, Phillips RJ. 1988. Lunar composition: a geophysical and petrological synthesis. *J. Geophys. Res*. 93:6338–52

Nakamura Y. 1976. Seismic energy transmission in the lunar surface zone determined from signals generated by movement of lunar rovers. *Bull. Seismol. Soc. Am*. 66:593–606

Nakamura Y. 1977a. Seismic energy transmission in an intensely scattering environment. *J. Geophys. Res*. 43:389–99

Nakamura Y. 1977b. HFT events—shallow Moonquakes. *Phys. Earth Planet. Int.* 14: 217–23

Nakamura Y. 1978. A1 Moonquakes: source distribution and mechanisms. *Proc. Lunar Sci. Conf.* 9:3589–607

Nakamura Y. 1983. Seismic velocity structure of the lunar mantle. *J. Geophys. Res*. 88:677–86

Nakamura Y. 2003. New identification of deep Moonquakes in the Apollo lunar seismic

data. *Phys. Earth Planet. Int.* 139:197–205

Nakamura Y. 2005. Far-side deep Moonquakes and deep interior of the Moon. *J. Geophys. Res*. 110:E01001, doi: 10.1029/2004JE002332

Nakamura Y, Anderson DL. 1979. Martian wind activity detected by a seismometer at Viking lander 2 site. *Geophys. Res. Lett.* 6: 499–502

Nakamura Y, Dorman J, Duennebier F, Lammlein D, Latham G. 1975. Shallow lunar structure determined from the passive seismic experiment. *Moon* 13:57–66

Nakamura Y, Latham G, Lammlein D, Ewing M, Duennebier F, Dorman J. 1974. Deep lunar interior inferred from recent seismic data. *Geophys. Res. Lett*. 1:137–40

Nataf H, Ricard Y. 1996. 3SMAC: An a priori tomographic model of the upper mantle based on geophysical modeling. *Phys. Earth Planet. Int.* 95:101–22

Neal CR, Banerdt WB, Chenet H, Gagnepain-Beyneix J, Hood L, et al. 2004. The lunar seismic network: mission update. *Lunar Planet. Sci. Conf., 35th*, Abstr. No. 2093. Houston, TX: Lunar Planet. Inst.

Oberst J. 1987. Unusually high stress drop associated with shallow Moonquakes. *J. Geophys. Res.* 92:1397–405

Oberst J, Deuchler C, Wählisch M, Hauber E, Knapmeyer M, Spohn T. 2004. Where do the Mars quakes occur? *Eur. Geosci. Union* EGU04-A-02939 (Abstr.)

Oberst J, Mizutani H. 2002. A new inventory of deep Moonquake nests visible at Apollo 12 area. *Lunar Planet. Sci. Conf, 33th*, Abstr. No. 1704. Houston, TX: Lunar Planet. Inst.

Oberst J, Nakamura Y. 1987. Distinct meteoroid families identified on the lunar seismograms. *J. Geophys. Res*. 92:E769–73

Oberst J, Nakamura Y. 1991. A search for clustering among the meteoroid impacts detected by the Apollo lunar seismic network. *Icarus* 91:315–25

Okal E, Anderson DJ. 1978. Theoretical models for Mars and their seismic properties *Icarus* 33:514–28

Phillips RJ. 1991. Expected rate of Marsquakes. In *Scientific Rationale and Requirements for a Global Seismic Network on Mars*, LPI Tech. Rep. 91–02, pp. 35–38. Houston: Lunar Planet. Inst.

Press F, Buwalda P, Neugebauer M. 1960. A lunar seismic experiment. *J. Geophys. Res*. 65:3097–105

Rhie A, Romanowicz B. 2004. Excitations of the Earth's incessant free oscillation by atmosphere/ocean/solid Earth coupling. *Nature* 431:552–56

Richardson JE, Melosh HJ, Greenberg R. 2004. Impact-induced seismic activity on asteroid 433 Eros: a surface modification. *Science* 306:1526–29

Righter K, Walker RJ, Warren PH. 2000. Significance of highly siderophile elements and osmium isotopes in the Lunar and terrestrial mantles. See Canup & Righter 2000, pp. 291–322

Ringwood AE, Essene E. 1970. Petrogenesis of Apollo 11 basalts, internal composition and origin of the Moon. *Apollo 11 Lunar Sci. Conf. Proc., Geochim. Cosmochim. Acta* 34:769–99

Sanloup C, Guyot F, Gillet P, Fei Y. 2002. Physical properties of liquid Fe alloys at high pressure and their bearings on the nature of metallic planetary cores. *J. Geophys. Res.* 107:doi: 10.1029/2001JB000808

Sanloup C, Jambon A, Gillet P. 1999. A simple chondritic model of Mars. *Phys. Earth Planet. Int.* 112:43–54

Sellers P. 1992. Seismic evidence for a low-velocity lunar core. *J. Geophys. Res*. 97: 11,663–72

Sohl F, Hussmann H, Schwentker B, Spohn T, Lorenz RD. 2003. Interior structure models and tidal Love numbers of Titan. *J. Geophys. Res*. 108:doi:10.1029/2003JE002044

Sohl F, Spohn T. 1997. The interior structure of Mars: implications from SNC meteorids. *J. Geophys. Res*. 102:1613–36

Sohl F, Spohn T, Breuer D, Nagel K. 2002. Implications from Galileo observations on the interior structure and chemistry of the Galilean satellites. *Icarus* 157:104–19

Solomon SC, Anderson DL, Banerdt WB, Butler RG, Davis PM, et al. 1991. Scientific rationale and requirements for a global nesimic network on Mars. *LPI Tech. Rpt. 91–02*, Lunar Planet. Inst., Houston, Tex. 51 pp.

Sotin C, Rocard F, Lognonné P. 2000. Summary of the internationnal conference of Mars exploration program and sample return mission. *Planet. Space Sci*. 48:1143–44

Spohn T, Sohl F, Breuer D. 1998. Mars. *Astron. Astrophys. Rev*. 8:181–236

Stegman DR, Richards M, Jellinek M, Manga M, Baumgardner J. 2004. Response of stagnant-lid convection to sudden dichotomy formation. Presented at Am. Geophys. Union, Spring Meet. Abstr. #P33B-04

Stevenson DJ. 2001. Mars' core and magnetism. *Nature* 412:214–19

Stofan ER, Saunders RS, Senske D, Nock K, Tralli D, et al. 1993. Venus interior structure mission (VISM): Establishing a seismic network on Venus. *Lunar Planet. Inst., Worksh. Adv. Technol. Planet. Instr.*, Part 1, pp. 23–24 (SEE N93-28764 11-91). Houston, TX: Lunar Planet. Inst.

Suda N, Mitani C, Kobayashi N, Nishida K. 2002. Theoretical calculation of Mars' background free oscillations. *Am. Geophys. Union, Fall Meet.*, Abstr. #S12A-1186, San Francisco

Surkov Y.1989. *Exploration of Terrestrial Planets from Spacecraft*, pp. 372–73. New York: Ellis Horwood. 390 pp.

Tanimoto T. 2001. Continuous free oscillations: atmosphere-solid Earth coupling. *Annu. Rev. Earth Planet. Sci.* 29:563–84

Tanimoto T. 2005. The oceanic excitation hypothesis for the continuous oscillations of the Earth. *Geophys. J. Int*. 160:276–88, doi: 10.1111/j.1365-246X.2004.02484.x

Taylor SR. 1986. The origin of the Moon: geochemical considerations. In *Origin of the Moon*, ed. WK Hartmann, RJ Phillips, GJ Taylor, pp. 125–43. Houston, TX: Lunar Planet. Inst.

Taylor SR. 1987. The unique lunar composition and its bearing on the origin of the Moon. *Geochim. Cosmochim. Acta* 51:1297–309

Toksöz MN, Press F, Anderson K, Dainty A, Latham G, et al. 1972a. Lunar crust: structure and composition. *Science* 176:1012–16

Toksöz MN, Press F, Anderson K, Dainty A, Latham G, et al. 1972b. Velocity structure and properties of the lunar crust. *Earth Moon Planets* 4:490–504

Toksöz MN. 1974. Geophysical data and the interior of the Moon. *Annu. Rev. Earth Planet. Sci*. 2:151–77

Toksöz MN. 1975. Lunar and planetary seismology. *Rev. Geophys. Space Phys.* 13: 306

Toksöz MN. 1979. Planetary seismology and interiors. *Rev. Geophys. Space Phys.* 17: 1641–55

Toksöz MN, Dainty AM, Solomon SC, Anderson KR. 1974. Structure of the Moon. *Rev. Geophys. Space Phys*. 12:539–67

Yoder CF, Konopliv AS, Yuan DN, Standish EM, Folkner WM. 2003. Fluid core size of Mars from detection of the solar tide. *Science* 300:299–303

Vinnik L, Chenet H, Gagnepain-Beyneix J, Lognonné P. 2001. First seismic receiver functions on the Moon. *Geophys. Res. Lett.* 28:3031–34

Van Hoolst T, Dehant V, Roosbeek F, Lognonné P. 2003. Tidally induced surface displacements, external potential variations, and gravity variations on Mars. *Icarus* 161:281–96

Verhoeven O, Rivoldini A, Vacher P, Mocquet A, Choblet G, et al. 2004. Planetary interiors structure inferred from electromagnetic, geodetic and seismic network science. I: Forward problem and the case of Mars. *J. Geophys. Res*. In press

Walker JD, Huebner WF. 2004. Seismological investigation of asteroid and comet interiors. In *Mitigation of Hazardous Impacts Due to Asteroids and Comets*, ed. MJS Belton, DK Yeomans, TH Morgan, 234:265. Cambridge, UK: Cambridge Univ. Press

Wieczorek MA, Zuber MT. 2004. Thickness of

the Martian crust: Improved constraints from geoid-to-topography ratios. *J. Geophys. Res.* 109:doi: 10.1029/2003JE002153

Williams JG, Boogs DH, Yoder CF, Racliff JT, Dickey JO. 2001. Lunar rotational dissipation in solid body and molten core. *J. Geophys. Res.* 106:27933–68

Zharkov VN, Gudkova TV. 1997. On the dissipative factor of Martian interiors. *Planet. Space Sci.* 45:401–7

Zharkov VN, Gudkova TV. 2000. Interior structure models, Fe/Si ratio and parameters of figure for Mars. *Phys. Earth Planet. Int.* 117:407–20

Zuber MT. 2001. The crust and mantle of Mars. *Nature* 412:237–44

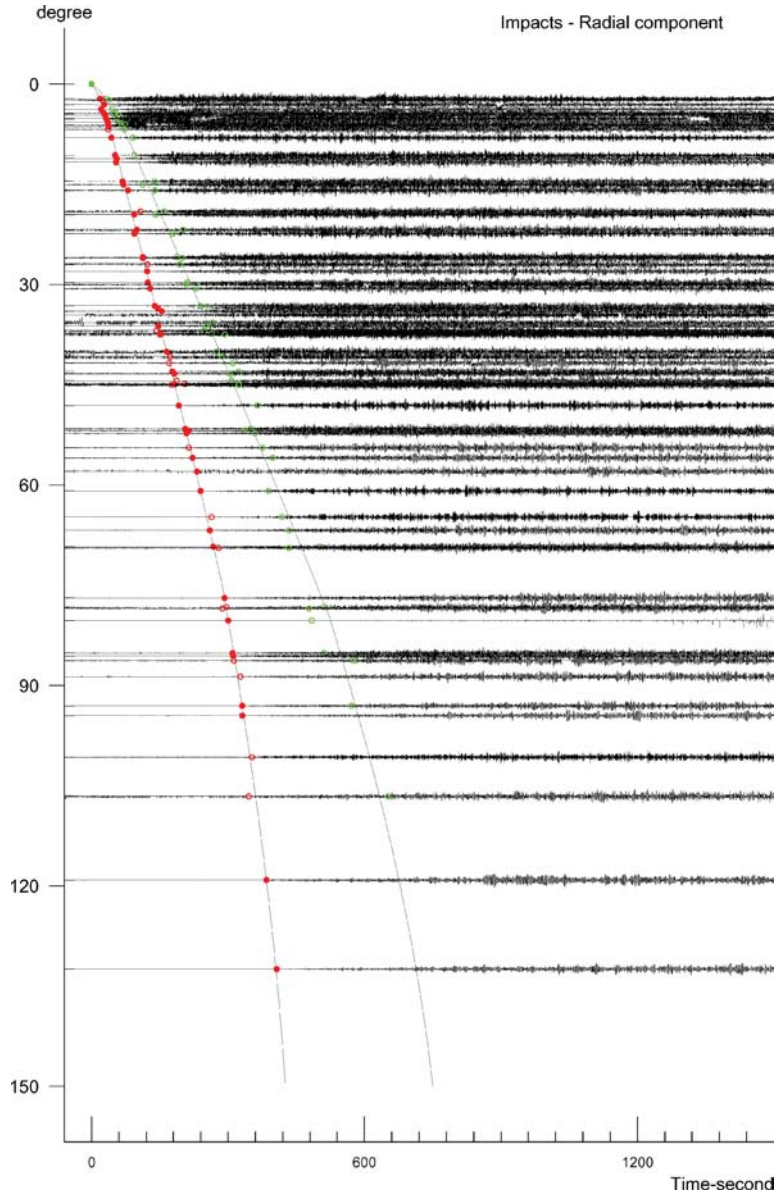

Figure 2 Profile of the vertical component of the meteoroid impacts, as listed and used by Lognonné et al. (2003). Note that a few of these events were observed at epicentral distances greater than 90°, including a few with more than 120°. Red circles are the P arrival times and green circles are for the S arrival times. Time is in seconds.

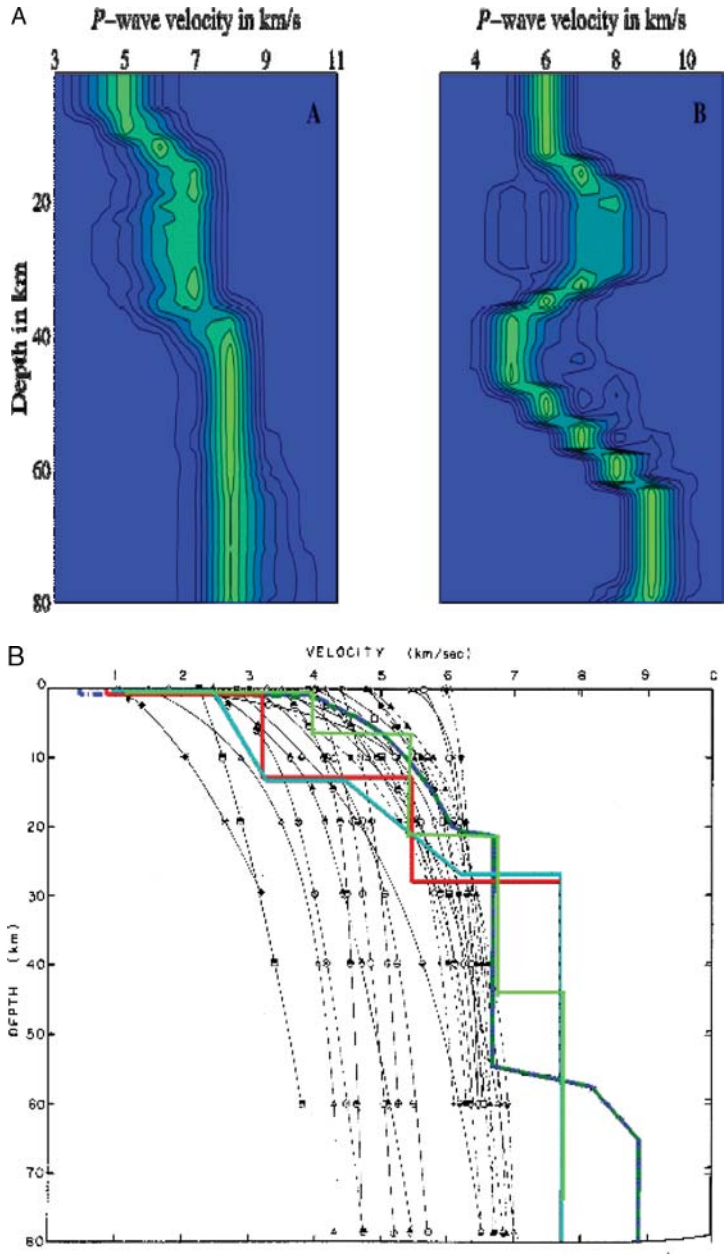

See legend on next page

Figure 4 (*a*) Crustal models from Khan & Mosegaard (2002) for a crust in the range of 40 ± 5 km (*A*) and in the range of 60 ± 10 km (*B*). As seen in the figure, the models found in case *A* correspond to a more realistic structure from a geophysical point of view. The upper part of the crust–to-mantle transition for the models in case *A* is located at a depth of 38 ± 3 km. (*b*) Crustal models of Toksöz (1974) (*dark blue line*), of Lognonné et al. (2003) (*red* and *light blue lines*), and of Koyama & Nakamura (1979) (*green line*). The crust/mantle discontinuity is, respectively, 65 km, 30 km, and 45 km deep and velocities below are those of the mantle. In the background are the seismic velocities extrapolated from crustal lunar samples after Toksöz (1974). Toksöz (1974) and Koyama and Nakamura (1979) velocities in the crust between 30 and 60 km are high with respect to the extrapolated velocities.

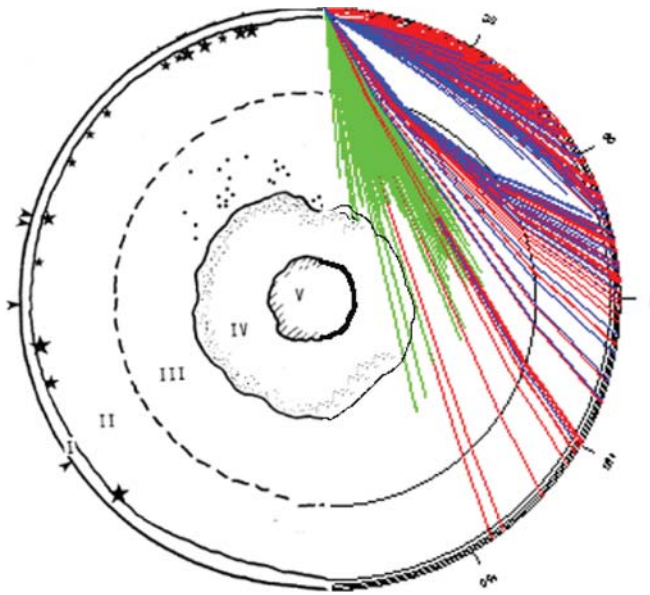

Figure 6 Left hemisphere: Polar view of the Moon with the distribution of the stations (*squares*) and the deep interior structure after Nakamura (1983). The stars are for shallow Moonquakes, whereas the dots are for deep Moonquakes. Green, blue, and red rays are for deep quakes, shallow quakes, and impact meteoroids, respectively. Areas I, II, III, IV, and V are the crust, upper mantle, middle mantle, lower mantle, and core, respectively. Right hemisphere: Plot of all rays used by Lognonné et al. (2003). Rays are shown for a hypothetical station for simplicity, and their three-dimensional distribution is not taken into account. The core is not covered by any ray and only a few propagate through the deep lower mantle.

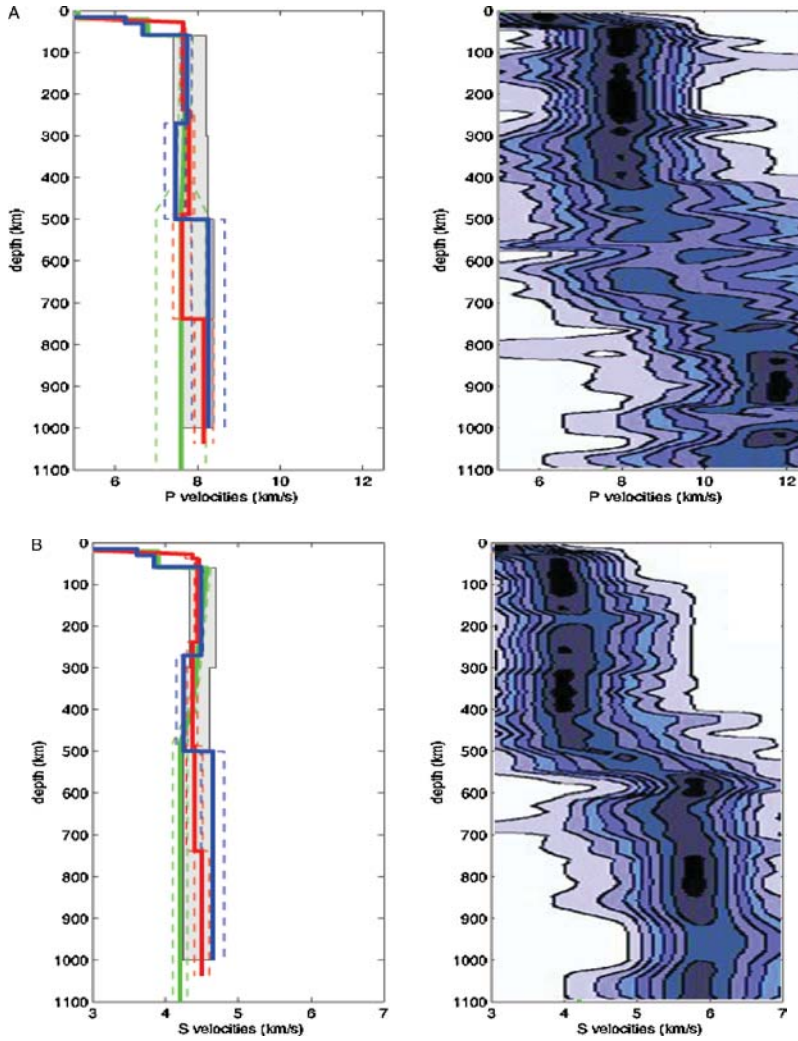

Figure 5 (*a*) Mantle models of the Moon for P velocities. Left figure shows the layered models of Goins et al. (1981c) (*green*), Nakamura (1983) (*blue*), and Lognonné et al. (2003) and Gagnepain-Beyneix et al. (2004) (*red*). The gray zone is for geochemical admissible models, following Kuskov et al. (2002). The dashed lines are associated to the error bars of the models. Right figure shows the probability distributions of Khan et al. (2002), with contours describing nine equal-sized probability density intervals. (*b*) Same as (*a*) for S velocities. All models have large errors and the latter must be taken into account in the interpretation of seismic velocities in terms of mineralogy and interior structure.

Annual Review of Earth and Planetary Sciences
Volume 33, 2005

CONTENTS